Annals of Physics 324 (2009) 1953–1982

Contents lists available at ScienceDirect

Annals of Physics

journal homepage: www.elsevier.com/locate/aop

Dynamical manifestations of Hamiltonian monodromy

J.B. Delos [a,*], G. Dhont [b], D.A. Sadovskií [b], B.I. Zhilinskií [b]

[a] Physics Department, College of William and Mary, Williamsburg, VA 23185, USA
[b] Département de physique, UMR 8101 du CNRS, Université du Littoral Côte d'Opale, 59140 Dunkerque, France

ARTICLE INFO

Article history:
Received 30 January 2009
Accepted 16 March 2009
Available online 24 March 2009

PACS:
45.05.+x
45.50.−j
03.65.Sq

Keywords:
Hamiltonian monodromy
Energy–momentum map

ABSTRACT

Monodromy is the simplest obstruction to the existence of global action–angle variables in integrable Hamiltonian dynamical systems. We consider one of the simplest possible systems with monodromy: a particle in a circular box containing a cylindrically symmetric potential-energy barrier. Systems with monodromy have nontrivial smooth connections between their regular Liouville tori. We consider a dynamical connection produced by an appropriate time-dependent perturbation of our system. This turns studying monodromy into studying a physical process. We explain what aspects of this process are to be looked upon in order to uncover the interesting and somewhat unexpected dynamical behavior resulting from the nontrivial properties of the connection. We compute and analyze this behavior.

1. Introduction

The system we examine [1] is a classical particle of mass μ moving in two dimensions $\mathbf{q} = (x, y)$ without friction inside a circular box of radius $\rho_{\max}$ on a cylindrically symmetric potential-energy barrier

$$V(\mathbf{q}) = -\frac{1}{2}a\mathbf{q}^2 \quad \text{when } \rho \equiv |\mathbf{q}| \leqslant \rho_{\max} \tag{1a}$$

$$= \infty \quad \text{when } \rho > \rho_{\max} \tag{1b}$$

with $a > 0$. The particle will be subjected to additional perturbations; its unperturbed Hamiltonian is

* Corresponding author.
E-mail addresses: jbdelo@wm.edu (J.B. Delos), guillaume.dhont@univ-littoral.fr (G. Dhont), sadovski@univ-littoral.fr (D.A. Sadovskií), zhilin@univ-littoral.fr (B.I. Zhilinskií).

0003-4916/$ - see front matter © 2009 Elsevier Inc. All rights reserved.
doi:10.1016/j.aop.2009.03.008

$$H_0(\mathbf{q},\mathbf{p}) = \frac{1}{2\mu}(p_x^2 + p_y^2) + V(\mathbf{q}) \tag{2}$$

where $\mathbf{q} = (x, y)$ and $\mathbf{p} = (p_x, p_y)$ are canonically conjugate Cartesian coordinates and momenta of the particle. Throughout this paper, we will assume [2]

$$\mu = a = 1 \tag{3a}$$

and unless noted explicitly otherwise, we will use

$$\rho_{\max} = 3 \tag{3b}$$

for all numerical examples.

The unperturbed motion under H_0 is simple: between specular reflections from the hard wall at $\rho = \rho_{\max}$ which reverse the radial component p_ρ of momentum $\mathbf{p}$, the particle travels up, scatters off, and descends the potential-energy hill. Between bounces, the trajectory $t \mapsto (\mathbf{q}(t), \mathbf{p}(t))$ is described by linear equations. A typical unperturbed trajectory is shown in Fig. 1. Energy $H_0(\mathbf{q}(t), \mathbf{p}(t))$ and angular momentum

$$M = \mathbf{q}(t) \times \mathbf{p}(t) = x(t)p_y(t) - y(t)p_x(t) \tag{4}$$

of the particle are conserved:

$$M(\mathbf{q},\mathbf{p}) = m, \quad H_0(\mathbf{q},\mathbf{p}) = E \geqslant \frac{m^2}{2\mu\rho_{\max}^2} - \frac{a}{2}\rho_{\max}^2 =: E_{\min}(m) \tag{5}$$

where (m, E) are constants. Throughout this paper, the letter E and the word 'energy' refer to the value of the unperturbed Hamiltonian $H_0(\mathbf{q},\mathbf{p})$. Also, following conventions that have arisen in this field, angular momentum is simply called 'momentum'. Since this system with two degrees of freedom has two conservation laws (5) and the motion is bounded in the phase space $\mathbb{R}^4$ with coordinates (x, y, p_x, p_y), we expect (by the Liouville–Arnol'd theorem [3]) that the trajectories formed at each fixed regular value (m, E) fill typically a 'torus' $\Lambda_{(m,E)}$ [23], and the family of such tori in the neighborhood of $\Lambda_{(m,E)}$ can be described by local action–angle variables. The origin $(m, E) = (0, 0)$ is a critical value which represents the unstable equilibrium together with its stable and unstable manifolds, so that the full preimage of $(0, 0)$ is a singular two-dimensional variety $\Lambda_{(0,0)}$ called a *pinched* torus [23].

The full dynamical flow φ of the perturbed system is generated by the vector field

$$X = X_{H_0} + X_1 \tag{6}$$

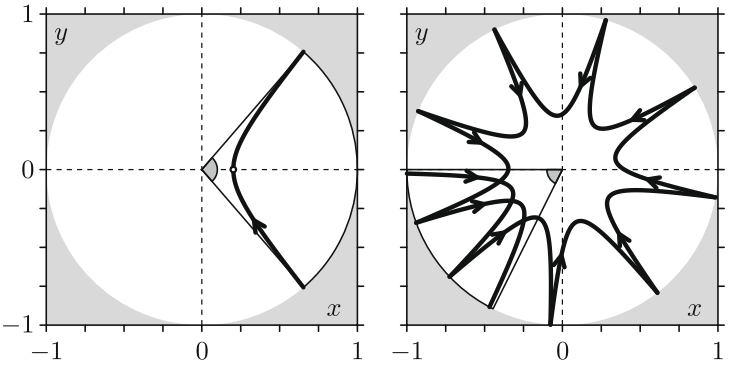

Fig. 1. Left: The (x, y)-trace of a reference orbit with angular momentum $m > 0$ (bold line), its pericenter (empty circle), and corresponding rotation angle θ (small shaded sector at the origin). Right: A trajectory bouncing around the cylindrical barrier: the coordinate image of the trajectory with $m = 0.1$, $E = -0.1$, and initial position on the wall just below the negative x axis. Small shaded sector at the origin indicates the total swept polar angle modulo 2π. Axes x and y are scaled in units of $\rho_{\max} = \sqrt{2}$; $\mu = a = 1$.

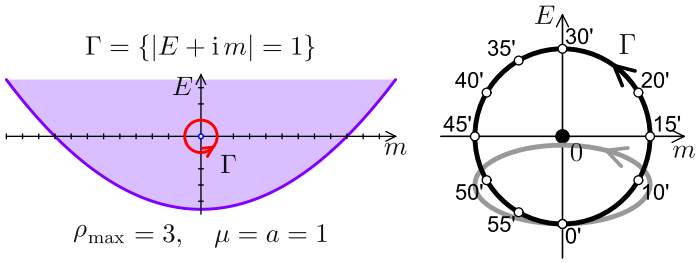

Fig. 2. Left: A monodromy circuit Γ (bold red) defined by (7) within the set of the regular values (shaded area) of the $\mathcal{EM}$ map of the system with Hamiltonian H_0 in (2). Right: Zoomed part near the monodromy center (0,0) with Γ (bold black) and 'placebo circuit' (bold gray); points on Γ are marked counterclockwise in 'minutes', $0' \ldots 60'$, starting with $m = 0$ and $E < 0$. (For interpretation of the references to color in this figure legend, the reader is referred to the web version of this paper.)

where X_{H_0} is the linear vector field defined by H_0 in (2) and the perturbing field X_1 will be described in more detail later. Its main required property [1] is that it causes the particle to change its energy and angular momentum continuously in time, so that if we monitor $E(t)$ and $m(t)$, we find that they go counterclockwise around a circuit Γ in the (m, E) plane encircling the origin (0,0) as shown in Fig. 2.

The unperturbed system described by Hamiltonian H_0 in (2) is one of the simplest examples of systems with nontrivial monodromy [4]. In such a system, as will be explained in more detail later, if we relate continuously the coordinates on the neighboring regular tori with energy E and angular momentum m while (m, E) follow a closed directed path Γ encircling (0,0), and then compare final and initial coordinates after completing one tour and returning to the same torus, we will find that the final and initial coordinates do not match.

In this paper, we analyze the dynamical consequence of this phenomenon, which we called "dynamical monodromy" [1]. In our case, the tori are connected dynamically by a (time-dependent) perturbation of the system. This turns studying topological monodromy into studying a physical process, i.e., a time evolution of a physical system whose (unperturbed) energy and angular momentum change and then return to their original values. Given that the underlying unperturbed system described by $H_0(\mathbf{q}, \mathbf{p})$ has interesting topological properties, the question is: what should we study in order to observe them? The answer to this question is our main objective. We show that monodromy of the unperturbed system leads to unexpected and nontrivial dynamical behavior of the perturbed system.

The paper is organized as follows. We begin in Section 2 by describing what happens to a certain family of trajectories if it is subjected to certain chosen perturbations. The family of trajectories begins and ends at a negative energy so that the allowed region of configuration space is an annulus. The set of initial conditions of the particles forms a loop in phase space which projects to a 'trivial' loop in the annulus. We show by computations that a passage around the monodromy circuit Γ carries particles to unexpected locations, so that the topology of the final loop in configuration space is different from that of the initial loop: the loop wraps around the forbidden region. In a previous short paper [1] we showed this behavior in a movie, and we urge the reader to read that reference and watch that movie before digging into the mathematical theory presented here. The purpose of this paper is to give a full analysis of this behavior.

In Section 3.1 we connect with quantum monodromy (which at present might be more familiar to some readers), and we give a brief discussion of different possible choices of classical actions and corresponding quantum numbers often used in systems with axial symmetry. Further in Section 3.2, we explain the monodromy of the 'static' system with Hamiltonian (2), and then in Section 3.3, we formulate the Hamiltonian monodromy theorem.

In Section 4 we return to the behavior of the perturbed classical system described in Section 2. We analyze how this behavior is related to changes of angle and action variables and to the monodromy of the unperturbed system. Subsequently, in Section 5, we turn to other possibilities to reveal monodromy in the perturbed system. Notation is defined in Table 1.

Table 1
Notation used throughout the paper.

$\mathbf{q} = (x, y)$	Cartesian coordinates in the configuration space
$\mathbf{p} = (p_x, p_y)$	Conjugate momenta
$\rho = \lvert\mathbf{q}\rvert$	Radius in the configuration space
$\rho_{\max}$	Fixed radius of the wall of the circular box
$\rho_{\min}(m, E)$	Radial position of the inner turning point
$\phi = \tan^{-1}\frac{y}{x}$	Polar angle
$a > 0$	Potential force constant (later set to 1 [2])
$\mu > 0$	Mass (later set to 1 [2])
$M = M(\mathbf{q}, \mathbf{p})$	Angular momentum (or simply *momentum*)
m	Value of M
$H_0(\mathbf{q}, \mathbf{p})$	Unperturbed Hamiltonian (2)
E	The value of H_0 called *energy*
$X_{H_0}(\mathbf{q}, \mathbf{p})$	Vector field defined by H_0
$\varphi_0^t(\mathbf{q}, \mathbf{p})$	Linear flow defined by X_{H_0}
$\mathcal{EM}$	Energy–momentum map with value (m, E)
$\mathbf{s} = (m, E)$	Point in the energy–momentum plane $\mathbb{R}^2$
$\Lambda_{(m,E)}$	Fiber of the $\mathcal{EM}$ map in $\mathbb{R}^4$
$\Lambda_{0,0}$	Singular fiber (pinched torus)
Γ	Monodromy circuit in the (m, E)-plane
$\tau(m, E)$	Period of first return
$\theta(m, E)$	Rotation angle
$\mathbf{J} = (J_1, J_2)$	Local action with values $\mathbf{j} = (j_1, j_2)$ [5]
$\mathbf{W} = (W_1, W_2)$	Conjugate local angles with values $\mathbf{w} = (w_1, w_2)$

2. The main result

Two ideas are central to this work [1]: (i) we define the perturbation implicitly by the resulting evolution of $\mathbf{s} = (m, E)$ and resulting perturbed trajectories and (ii) we study a *family* of trajectories, which we call 'particles', starting on a fundamental loop $\tilde{\gamma}(0)$ of a regular torus $\Lambda_{(m,E)}$.

Specifically we assume that under this perturbation, energy–momentum values $\mathbf{s}$ follow along circuit Γ (Fig. 2) which we choose here as

$$\Gamma : [0, 60] \to \mathbb{R}^2 : t \mapsto \mathbf{s}(t) = \begin{pmatrix} \sin \Omega t \\ -\cos \Omega t \end{pmatrix} \tag{7}$$

with $\Omega = 2\pi/60$. The concrete choice of Γ is not important as long as it encircles the origin $\mathbf{s} = 0$ and lies entirely in the set of regular $\mathcal{EM}$ values; for Eq. (7) this can be verified using Fig. 2. Furthermore, we assume that at any instant t, all particles have the same value $\mathbf{s}(t)$, i.e., all particles are located on the same torus $\Lambda_{\mathbf{s}(t)}$ of the unperturbed system. So at the initial time $t = 0$ they begin on $\Lambda_{\mathbf{s}(0)}$ with $m = 0$ and $E = -1$ and then they come back to this torus at $t = 60$.

On regular tori $\Lambda_{(m,E)}$, we have two basic closed directed paths γ_1 and γ_2, which represent two classes $[\gamma_1]$ and $[\gamma_2]$ of the fundamental group π_1 of $\Lambda_{(m,E)}$ [6]. They are given explicitly in [1] and we will return to this construction later in Section 4.1.5. One path, γ_1 is *fixed* on all tori as an orbit of the Hamiltonian flow of the vector field X_M generated by the Hamiltonian function $M(\mathbf{q}, \mathbf{p})$; it can be specified as the loop $0 \leqslant \phi \leqslant 2\pi,\ \rho = \rho_{\max}$. The other path $\gamma_2 = \gamma_2(t) \subset \Lambda_{\mathbf{s}(t)}$ must be defined *smoothly* as $\mathbf{s}(t)$ follows Γ. Initially it can be defined to be a loop where the torus intersects $y = 0$ with the restriction $x > 0$.

In [1], particles were started on $\tilde{\gamma}(0) = \gamma_2(0)$ with $y = p_y = 0$ and with variables x and p_x consistent with $(m, E) = (0, 0)$. The perturbation was assumed such that particles followed unperturbed trajectories $t \mapsto (\mathbf{q}(t; m, E), \mathbf{p}(t; m, E))$ whose parameters (m, E) varied along Γ. Here we start particles in the same way, but instead of working in the $(\mathbf{q}, \mathbf{p})$ phase space $\mathbb{R}^4$ we consider the flow of our system in local action–angle coordinates $(\mathbf{J}, \mathbf{W})$ [5], which exist in a sufficiently small open neighborhood of any regular torus $\Lambda_{(m,E)}$. In these coordinates, trajectories of the unperturbed system with Hamiltonian

H_0 in (2) are described as follows. Starting at some initial point $\mathbf{w}(0)$ on $\Lambda_{(m,E)}$ (see Fig. 8), they evolve linearly and wind around the torus according to

$$\mathbf{w}(t) = \mathbf{w}(0) + \boldsymbol{\nu}(m,E)t \tag{8}$$

where $\boldsymbol{\nu}(m,E)$ are characteristic frequencies on $\Lambda_{(m,E)}$. Furthermore, functions

$$\mathcal{J}(m,E) = (\mathcal{J}_1(m,E), \mathcal{J}_2(m,E)) = (2\pi m, \mathcal{J}_2(m,E))$$

which relate the values $\mathbf{j}$ of $\mathbf{J}$ to the energy and momentum, [7] and which are given by integrating $\mathbf{p}\,d\mathbf{q}$ along γ_1 and γ_2, respectively, are *locally* smooth real single-valued functions.

Let us assume here that our perturbation causes the values of local actions $\mathcal{J}$ to vary in time so that corresponding (m,E) follow Γ while the values of local angles $\mathbf{w}$ evolve in the same way as for the unperturbed system, i.e., according to Eq. (8) with varying (m,E). We call this perturbation *ideal*. Under such a perturbation, what is the evolution of the loop $\tilde{\gamma}(t)$ which represents the phase space positions of particles at time t? We observe in Fig. 3 the evolution of $\tilde{\gamma}(t)$. We have

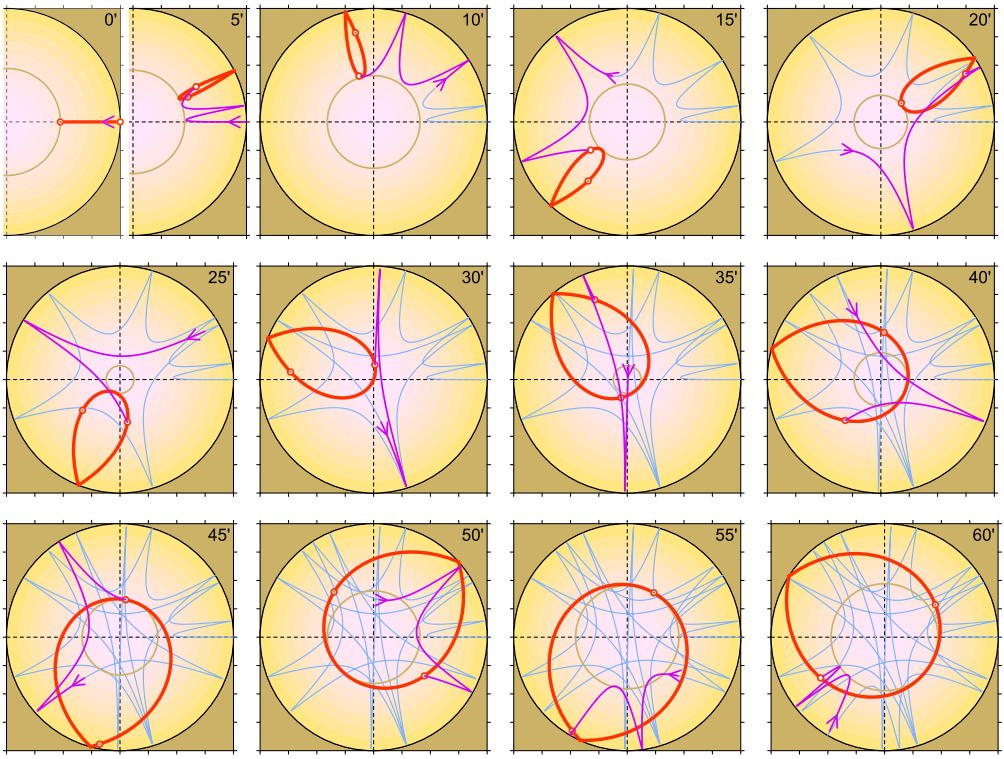

Fig. 3. Snapshots of the evolution of a closed continuous loop (bold line) in the (x,y)-plane representing the (x,y)-projection of instantaneous phase-space positions of noninteracting particles which form a continuous one-parameter family and whose motion is governed by the vector field (6) with perturbing term X_1 so that their unperturbed energy E and momentum m evolve with time $t = 0\ldots60$ according to the monodromy circuit in Fig. 2 and Eq. (7). Current time t (in s) is indicated in the upper right corner of each plot. At all times, particles have the same (m,E) and lie at different points ξ on a particular cycle γ_2 defined in (36). Specifically, at $t = 0'$ (upper left plot), particles have $(m,E) = (0,-1)$ and lie on the cycle $\gamma_2(0')$ which projects on the segment $[\rho_{\min}, \rho_{\max}]$ of the positive semiaxis x; at $t = 60'$ all particles regain $(m,E) = (0,-1)$. Gray central circle marks the classically forbidden region for each t. Small empty circles and circles-with-a-dot mark instantaneous coordinates of particles I and II started at $t = 0'$ with $x = \rho_{\max}$ (at the wall, $\xi = \frac{1}{2}$) and $x = \rho_{\min}$ (at the pericenter, $\xi = 0$), respectively. Also shown is the (x,y)-projection (thin solid line) of the trajectory of particle I followed to the current time; the part of the trajectory added since the time of the preceding snapshot is highlighted.

Result 1. Under an ideal realization of the monodromy circuit Γ beginning in $\mathbf{s}(t_i)$ with $m = 0$ and $E < 0$ and ending in $\mathbf{s}(t_f) = \mathbf{s}(t_i)$, the loop $\tilde{\gamma}(t_i) = \gamma_2(0)$ evolves into a topologically different loop on the same torus $\Lambda_{\mathbf{s}(t_f)}$ at time $t = t_f$. The final loop at $\tilde{\gamma}(t_f)$ combines $\gamma_2(0)$ with γ_1 as $\tilde{\gamma}(t_f) = \gamma_2(0) - \gamma_1$. Its projection into the configuration space goes around the classically forbidden region surrounding the origin. This phenomenon is topological. It persists for a large class of realizations of Γ, called admissible, and for any loop of initial conditions which remains in a sufficiently small open regular neighborhood of $\Lambda_{\mathbf{s}(t_i)}$ and is homotopic to $\gamma_2(0)$ within this neighborhood.

The most striking aspect of the resulting evolution of our loop is that for the initial–final $\mathbf{s}(0) = \mathbf{s}(60) = (0, -1)$, there is a large classically forbidden region, a disk $\{|\mathbf{q}| < \rho_{\min}(m, E)\}$ whose boundary is shown by a circle in the center of each snapshot in Fig. 3. This region vanishes only when the instantaneous energy–momentum $\mathbf{s}(t)$ crosses the semiaxis $\{m = 0, E > 0\}$, and for all other $\mathcal{EM}$-values, unperturbed particles cannot enter it. Their allowed configuration space is an annulus $[\rho_{\min}, \rho_{\max}] \otimes \mathbb{S}^1$ in the $\mathbf{q}$ plane. Yet the initial loop is entirely on one side of the forbidden disk, while the final loop encircles it. In other words, these loops belong to different elements of the fundamental group of the annulus, i.e., different homotopy classes of closed paths in the allowed configuration space. The purpose of this paper is to explain this phenomenon.

3. Hamiltonian monodromy

Monodromy as a topological property of classical integrable Hamiltonian systems was introduced in [8]; its manifestations in corresponding quantum systems were described in [9–14]. Several simple mechanical systems [15], as well as a growing number of real fundamental physical systems, notably the hydrogen atom in external fields [16], the CO_2 molecule [17], the H_2O molecule [18], rotating dipolar molecules in an external electric field [19,20]—to name a few, are known to possess this property.

3.1. Smooth actions and corresponding quantum numbers

We begin by examining an even simpler system described by Hamiltonian H_0 in (2) with barrier parameter $a = 0$, i.e., a particle in a 'flat' circular box. We examine it first in quantum mechanics, and then we connect its quantum properties to properties of action variables.

The quantum energies $E_{n_\rho \hat{m}}$ and related values of the radial wave vector $k_{n_\rho \hat{m}}$ are labeled by integer quantum numbers $\hat{m}$ and n_ρ. Fig. 4a (left) shows the joint spectrum of discrete values (m, E) of angular momentum (4) and energy (2), conventionally called the *energy–momentum spectrum*. It can be approximated as

$$E_{n_\rho \hat{m}} = \frac{1}{2}\hbar^2 k^2_{n_\rho \hat{m}} \approx \frac{1}{8}\hbar^2 \left(n_\rho + \frac{1}{2}|\hat{m}| - \frac{1}{4}\right)^2 \rho^{-2}_{\max} \tag{9}$$

where $n_\rho = 1, 2, \ldots$ corresponds to what might be regarded as the "most natural" way to label the eigenfunctions. This n_ρ counts the number of radial nodes (including the one at $\rho_{\max}$) while $\hat{m}$ characterizes the angular behavior of the wavefunction.

In Fig. 4b (left) curves are drawn that go through points of fixed n_ρ. The slope of these lines is, obviously, *discontinuous* at $\hat{m} = 0$. Can we find a way to define the quantum numbers such that the connecting curves are smooth over the whole region of the spectrum? As illustrated in Fig. 4c–e (left), if we define quantum numbers

$$n_+ = n_\rho \quad \hat{m} \geqslant 0 \tag{10a}$$

$$n_+ = n_\rho - \hat{m} \quad \hat{m} \leqslant 0 \tag{10b}$$

or

Fig. 4. Comparison of a circular box system (left column) to a circular barrier system (right column), both with $\mu = 1$ and $\rho_{\max} = \frac{1}{4}$. Dots show quantum joint (m, E)-spectra for $\hbar = 1/40$; lines indicate constant level sets of classical action $\mathcal{J}_2(m, E)$ for different choices of J_2 (rows b–e). For the circular barrier (right), any path encircling once counterclockwise the monodromy center at the origin $(m, E) = 0$ represents the monodromy circuit Γ. Also shown (top right) is the result of the transport of a unit cell of the lattice of quantum states along Γ; the unit cell does not come back to itself.

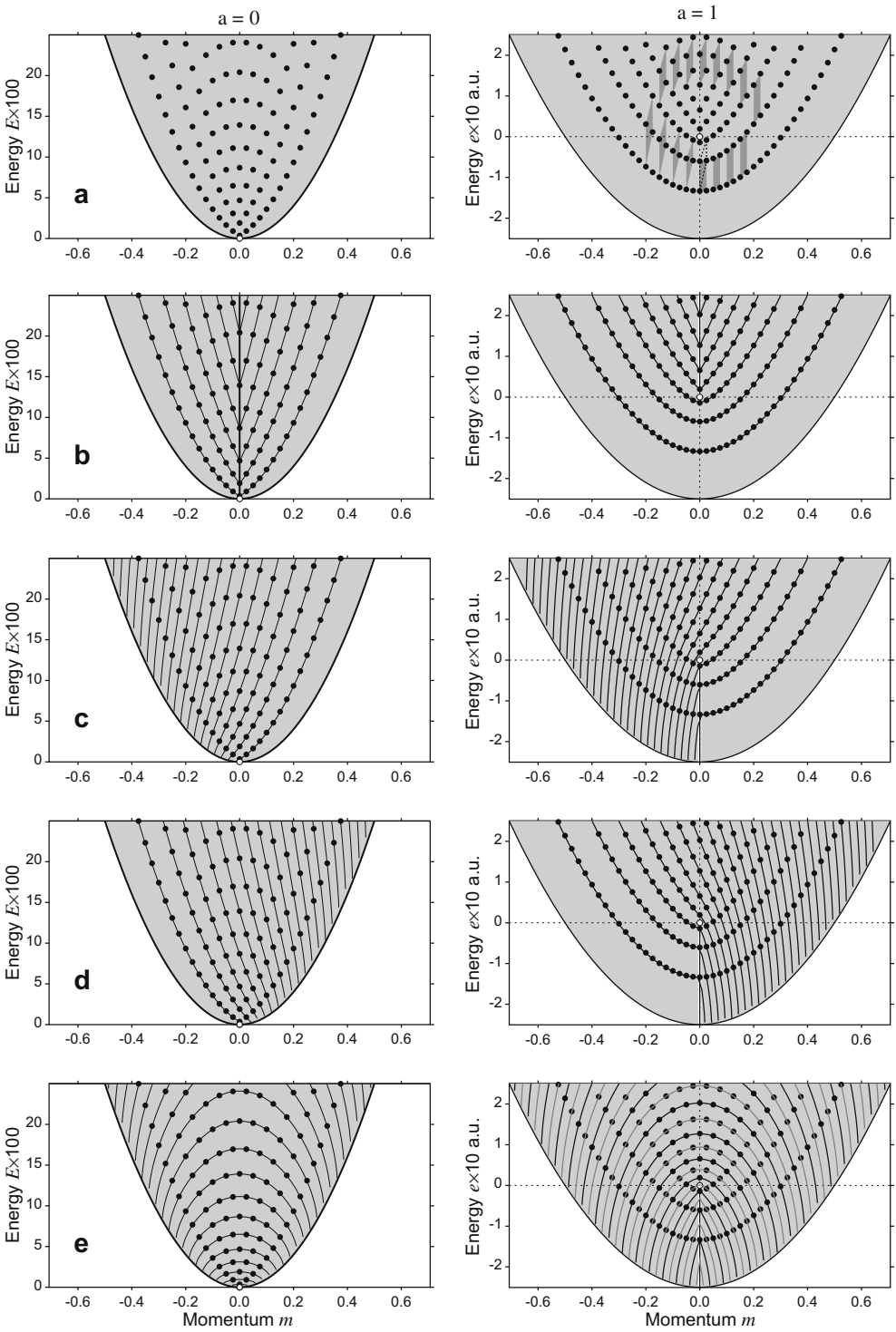
a = 0
a = 1
Energy $E\times100$
Energy $e\times10$ a.u.
a
b
c
d
e
Momentum m
Momentum m

$$n_- = n_\rho + \hat{m} \quad \hat{m} \geqslant 0 \tag{10c}$$
$$n_- = n_\rho \quad \hat{m} \leqslant 0 \tag{10d}$$

or

$$n_s = 2n_\rho + |\hat{m}| \tag{10e}$$

and construct curves connecting either states of fixed n_+ (Fig. 4c, left) or n_- (Fig. 4d, left) or n_s (Fig. 4e, left), then those curves are *globally smooth*. So it follows that the discontinuity or 'kink' of the curves in Fig. 4b, left, is related to our particular choice of quantum numbers.

The curves drawn in Fig. 4b–e correspond to quantized values of classical action variables, and the different structure of the curves follows from the fact that those action variables can be defined in several different ways. Because of the axial symmetry, one of them, $J_1 := 2\pi M$ can be chosen naturally using the (angular) *momentum* M in (4). Its conserved value $2\pi m$ is quantized as $2\pi\hat{m}\hbar$, with $\hat{m}$ integer. The second action variable may be defined in a number of ways. These choices can be explained by considering the values $\mathcal{J}_2(m,E)$ of this variable as function of (m,E) [7].

A seemingly natural (and most usual) choice would be to define the second action variable J_2 by a radial action integral

$$\mathcal{J}_2 : \stackrel{?}{=} \mathcal{J}^0_\rho(m,E) = 2\int_{\rho_{\min}(m,E)}^{\rho_{\max}} \mathcal{P}_\rho(\rho;m,E)\,d\rho \tag{11a}$$

where $\mathcal{P}_\rho(\rho;m,E)$ is defined as the positive square root

$$\mathcal{P}_\rho(\rho;m,E) = \sqrt{2\mu[E - V(\rho) - \frac{1}{2}m^2/(\mu\rho^2)]} > 0 \tag{11b}$$

and $\rho_{\min}(m,E)$ is the inner turning point of the radial motion. Contours (or constant level sets) of $\mathcal{J}^0_\rho(m,E)$ corresponding to its quantized values $2\pi\hbar(n^0_\rho + \frac{3}{4}), n^0_\rho \geqslant 0$ are the curves shown in Fig. 4b (left). Definition (11) makes $\mathcal{J}_2$ an even function of m. This is a natural choice from the perspective of time-reversal symmetry of the system with Hamiltonian (2) which acts as $m \to -m$. However, such a choice forces contours of $\mathcal{J}_2$ to have a kink at $m = 0$ where $\partial\mathcal{J}^0_\rho/\partial m$ is discontinuous [21].

Several other choices of the second action J_2 are available. We could take it to be either J_+, or J_-, or J_s, where

$$J_+ = J^0_\rho \quad J_- = J^0_\rho + 2\pi M \qquad M \geqslant 0 \tag{12a}$$
$$J_+ = J^0_\rho - 2\pi M \quad J_- = J^0_\rho \qquad M \leqslant 0 \tag{12b}$$
$$J_s = 2J^0_\rho + 2\pi|M| \tag{12c}$$

Quantizing the values of these action variables as

$$\mathcal{J}_\pm = 2\pi\hbar\left(n_\pm + \frac{3}{4}\right) \quad \text{and} \quad \mathcal{J}_s = 2\pi\hbar\left(n_s + \frac{3}{4}\right)$$

with integer $n_\pm \geqslant 0$ and $n_s \geqslant 0$ satisfying (10), and plotting contours in the (m,E) plane leads to the curves shown in Fig. 4c–d (left) and Fig. 4e (left), respectively. Note that $\mathcal{J}_s$ is an obvious alternative to $\mathcal{J}^0_\rho$ which is both even in m and smooth.

Is there a "best" definition of action variables and quantum numbers? That depends on the physical process being considered. So long as we are only interested in 'static' properties of individual eigenstates, J^0_ρ and n^0_ρ are a good choice, because they preserve the $m \to -m$ symmetry, and they count the radial nodes in the eigenfunctions. However, if we are concerned about dynamical processes, other choices might be better.

Let us consider transitions induced by radiation that is $(\pm)$ circularly polarized in the plane of the box. Of course such radiation perturbs the system and breaks its $m \to -m$ symmetry. Since quantum selection rules for $(\pm)$ radiation are $\Delta\hat{m} = \pm 1$ for absorption and $\Delta\hat{m} = \mp 1$ for emission, a sequence of such transitions may preserve either n_+ or n_-. Such a sequence would follow the contours of $\mathcal{J}_\pm$ as illustrated in Fig. 4 but *not* those of $\mathcal{J}^0_\rho$. So the numbers $n_\pm$ may give a simpler description.

The circular box system does not have monodromy, but it has some properties in common with other axially symmetric systems that do. It is perhaps the simplest system in which one naturally raises questions about how to define smooth actions and appropriate quantum numbers. Also it is structurally unstable. A small deformation with $a > 0$ converts it into a system that does have monodromy, and for which *no* smooth choice of actions and quantum numbers can be made globally. (A small deformation into the opposite direction $a < 0$ yields a structurally stable oscillator system without monodromy.)

3.2. Monodromy of the circular barrier system

Let us now examine briefly the quantum system with Hamiltonian in (2) and $a > 0$. Its spectrum is shown in Fig. 4, top right, followed by level plots for different possible choices of classical actions which are analogous to the one we discussed above (Section 3.1 and Fig. 4, left column).

Comparing to the circular box system, the first difference we note is that the origin $(0,0)$ is now an isolated critical energy–momentum value surrounded by regular values (m,E) (gray shaded area) [22]. In the circular box system, $(0,0)$ represented a particle at rest at any point of the box, i.e., an open disk $\{\rho < \rho_{\max}, \mathbf{p} = 0\}$ of equilibrium positions in the phase space $\mathbb{R}^4$. After the deformation into the circular barrier system, it represents an isolated singular fiber in $\mathbb{R}^4$ called a *pinched torus*, which is surrounded by regular tori [23].

The presence of such a critical value at $(0,0)$ changes qualitatively the level sets of actions. In the case of the traditional choice in Fig. 4b, the action J is smooth for $E < 0$, but it has a "kink" at $m = 0$ when $E > 0$. On the other hand, the "left" and "right" actions $J_\pm$ are both smooth when $E > 0$, but they have a discontinuous derivative on the half-line $\{m = 0, E < 0\}$. These singularities of actions reflect a real nontrivial physical property of the system—its *monodromy*. The critical value at $(0,0)$ makes finding a globally smooth single-valued action *impossible*.

In general, actions J and corresponding action integrals $\mathcal{J}$ in systems with monodromy are *multivalued*. In our system, $\mathcal{J}_1 = 2\pi m$ is defined globally and is single valued. However (as pointed out by Vũ Ngọc [24,10]) the multivalued part of the second action $\mathcal{J}_2(m,E)$ near $(0,0)$ can be approximated as

$$m \arg(E + \mathrm{i}m) \tag{13}$$

Using different leaves of this function results in different $\mathcal{J}_2$. Since for any such choice, the values of arg have to sweep a full circle around $(0,0)$, any such action is not C_1-smooth in the regular open neighborhood of the singularity at $(0,0)$. Thus in particular, if we choose to start the leaf on the half-line $\{m = 0, E < 0\}$ and continue it smoothly around $(0,0)$ while increasing the value of arg, we come back with the *same* value j_2 but with a *different* $\partial\mathcal{J}_2/\partial m$. One can verify that the level sets of such $\mathcal{J}_2$ near $(0,0)$ are qualitatively equivalent to those in Fig. 4e, right. These sets are smooth for $E > 0$ and have a kink on $\{m = 0, E < 0\}$. Alternatively, we can start the leaf on $\{m = 0, E > 0\}$, and have level sets with a kink on this half-line (Fig. 4b). Two more possibilities with discontinuous first derivative $\partial\mathcal{J}_2/\partial m$ are represented in Fig. 4c and d. On the other hand, in all other cases, $\mathcal{J}_2(m,E)$ itself is discontinuous [25].

The corresponding joint (m,E) eigenvalue lattice of quantum states has a *defect* at $(0,0)$. The best way to characterize this defect is by choosing an elementary cell of this lattice and transporting it in small steps along a circuit around $(0,0)$. As can be seen in Fig. 4, top right, the deformation of the cell at each step is unambiguously defined by the two basis vectors of the cell. As we come back after completing a tour, the cell does not come back to itself. For any such lattice of quantum eigenvalues, neither n, nor $n_\pm$ or any other second quantum number is well defined globally.

As we will see in Section 3.3, this process of following a unit cell of a lattice of quantum eigenvalues corresponds to following smooth connections of action variables on classical tori.

3.3. Monodromy theorem

We summarize the preceding discussion in a more formal way. The first integrals (M, H_0) in (2) and (4) define the energy–momentum map

$$\mathcal{EM} : \mathbb{R}^4 \to \mathbb{R}^2 : (\mathbf{q},\mathbf{p}) \to (M(\mathbf{q},\mathbf{p}), H_0(\mathbf{q},\mathbf{p})) = (m,E)$$

Regular values (m,E) of the $\mathcal{EM}$ map are those for which the rank of the Jacobi matrix $\partial(M,H_0)/\partial(\mathbf{q},\mathbf{p})$ is 2 [22]; the corresponding regular fibers $\Lambda_{(m,E)}$, i.e., inverse images $\mathcal{EM}^{-1}(m,E)$ are tori [23]. The fiber $\Lambda_{0,0}$ is a pinched torus [23]: its pinch point $\mathbf{p}=\mathbf{q}=0$ is the critical point of the $\mathcal{EM}$ map at which the rank drops to 0; other points of $\Lambda_{0,0}$ are regular. Such an isolated critical fiber causes monodromy [26].

The set D^* of all regular $\mathcal{EM}$ values is an open domain in $\mathbb{R}^2$, shown as a gray shaded area in Fig. 4a, right. We can see that it is a punctured disk $D\setminus(0,0)$ which is not simply connected. In particular, any closed path Γ in D^* that circles once around (0,0) is non-contractible. By convention, Γ is directed counterclockwise, see Fig. 2. We call Γ a *monodromy circuit*, and we call (0,0) the *monodromy center*. Any contractible circuit in D^*, i.e., any circuit homotopic to a point, will be called a *placebo circuit*. Monodromy and placebo circuits represent two different elements of the fundamental group $\pi_1(D^*)$ [27].

In the neighborhood of any regular torus $\Lambda_{(m,E)}$ we can define local action and angle variables J_k and W_k with $k=1,2$, which we will denote by capital letters when we consider them as functions on the phase space. The *numerical values* of J_k and W_k are denoted by lower-case letters j_k and w_k. Boldface letters will refer to pairs, such as $\mathbf{J}=(J_1,J_2)$, $\mathbf{j}=(j_1,j_2)$ [5].

Consider now a bundle of regular tori $\Lambda_{(m,E)}$ over Γ. Action and angle variables can be defined for each $\Lambda_{(m,E)}$, and as we follow Γ and go continuously from a point on one torus to a point on another, the values $\mathbf{j}$, $\mathbf{w}$ of these variables change continuously [28]. For each fixed regular (m,E) and fixed (w_1,w_2), the relationships $W_1=w_1$ or $W_2=w_2$ define on $\Lambda_{(m,E)}$ two closed curves γ_2 and γ_1, respectively—the two fundamental loops of this torus. Directing them according to increasing angles (w_1,w_2) we obtain a cycle basis $(\gamma_1,\gamma_2)_{(m,E)}$ of the first homology group of $\Lambda_{(m,E)}$,—basically, a coordinate system on this torus. Furthermore, using the continuity properties of local actions and extending this definition to the neighboring tori, we obtain a continuous *connection* between them which relates their cycle bases continuously.

Let us begin building our connection at some initial point Γ_i of the monodromy circuit. There we have basis cycles $(\gamma_1,\gamma_2)_\mathrm{i}$. After one tour we arrive at $\Gamma_\mathrm{f}=\Gamma_\mathrm{i}$ with a *new* basis $(\gamma_1,\gamma_2)_\mathrm{f}$. Furthermore, let us choose $J_1=2\pi M$ and γ_1 as the trajectory γ_M of the system with Hamiltonian M, the generator of the axial symmetry. Then a general monodromy theorem [8,26,9,15,29] tells us that the initial and final cycle bases will not be the same. For our choice of cycle basis

$$\begin{pmatrix}\gamma_1\\ \gamma_2\end{pmatrix}_\mathrm{f}=\begin{pmatrix}1 & 0\\ -1 & 1\end{pmatrix}\begin{pmatrix}\gamma_1\\ \gamma_2\end{pmatrix}_\mathrm{i} \tag{14}$$

The *monodromy matrix* defining this transformation is a matrix in $\mathrm{SL}(2,\mathbb{Z})$. On the other hand, starting at the same regular torus $\Lambda_{\Gamma_\mathrm{i}}$ and following any placebo circuit (such as shown by the gray path in Fig. 2), we will obtain a trivial cycle basis bundle with $(\gamma_1,\gamma_2)_\mathrm{f}=(\gamma_1,\gamma_2)_\mathrm{i}$.

This result is independent of any particular choice of the monodromy circuit within the class of homotopic paths in D^*. Neither does it depend on the initial–final point, nor on a particular construction of the cycle bases and connections: the monodromy matrix in (14) remains the same up to a conjugation within $\mathrm{SL}(2,\mathbb{Z})$. Furthermore, since actions and cycles change in the same way (the values of actions are integrals along the cycles)

$$\begin{pmatrix}J_1\\ J_2\end{pmatrix}_\mathrm{f}=\begin{pmatrix}1 & 0\\ -1 & 1\end{pmatrix}\begin{pmatrix}J_1\\ J_2\end{pmatrix}_\mathrm{i} \tag{15}$$

and consequently, J_2 cannot be defined globally on $\mathcal{EM}^{-1}(D^*)$ as a real smooth single-valued function.

At the same time, pulling back J_k with $k=1,2$ by $\mathcal{EM}^{-1}$ and considering locally smooth single-valued real functions $\mathcal{J}_k$ of (m,E) on D^* [7], we observe that the Jacobian matrix

$$D\mathcal{J}(m,E)=\begin{pmatrix}\dfrac{\partial\mathcal{J}_1}{\partial m} & \dfrac{\partial\mathcal{J}_1}{\partial E}\\ \dfrac{\partial\mathcal{J}_2}{\partial m} & \dfrac{\partial\mathcal{J}_2}{\partial E}\end{pmatrix}_{(m,E)}$$

transforms as

$$D\mathcal{J}_{\rm f} = \begin{pmatrix} 1 & 0 \\ -1 & 1 \end{pmatrix} D\mathcal{J}_{\rm i} \tag{16}$$

[use the covector transformation property for gradients].

Quantum energy–momentum values correspond (within the semiclassical approximation) to quantized values of $(\mathcal{J}_1, \mathcal{J}_2)$ and it can be seen that the inverse transpose of $D\mathcal{J}(m,E)$ defines the elementary cell of the locally regular two-dimensional quantum lattice at point (m,E) in D^* [30]. Furthermore, it can be verified by a computation [9,10,31,32] that the respective transformation of the two basis vectors (v_1, v_2) defining the elementary cell at $(m,E)_{\rm f} = (m,E)_{\rm i}$, is given by the inverse transpose monodromy matrix

$$\begin{pmatrix} v_1 \\ v_2 \end{pmatrix}_{\rm f} = \begin{pmatrix} 1 & 1 \\ 0 & 1 \end{pmatrix} \begin{pmatrix} v_1 \\ v_2 \end{pmatrix}_{\rm i} \tag{17}$$

Finally, if the transformation in (15) is a symplectomorphism, conjugate angles (W_1, W_2) should also change like vectors (v_1, v_2) in (17)

$$\begin{pmatrix} W_1 \\ W_2 \end{pmatrix}_{\rm f} = \begin{pmatrix} 1 & 1 \\ 0 & 1 \end{pmatrix} \begin{pmatrix} W_1 \\ W_2 \end{pmatrix}_{\rm i} \tag{18}$$

The latter should be restated in both 'passive' and 'active' form. If we take a given point $(\mathbf{q}_{\rm i}, \mathbf{p}_{\rm i})$ on the initial torus $\Lambda_{\rm i}$, having values of angle variables (defined in the initial angle coordinate system) equal to $\mathbf{w}_{\rm i} = (w_1, w_2)_{\rm i}$, then, upon traversing once around the monodromy circuit, the coordinate functions W change so that the same point on the torus $(\mathbf{q}_{\rm i}, \mathbf{p}_{\rm i})$ is identified in the final coordinates by values

$$\mathbf{w}_{\rm final} = \begin{pmatrix} 1 & 1 \\ 0 & 1 \end{pmatrix} \mathbf{w}_{\rm i} \tag{19a}$$

Correspondingly, if we traverse a monodromy circuit, moving from one torus to another with the *numerical values* $\mathbf{w}$ of angle variables $\mathbf{W}$ held fixed, $\mathbf{w} = \mathbf{w}_{\rm i}$, then we do not come back to the original point on the torus. The new point to which we return is defined in the old coordinates as

$$\mathbf{w}_{\rm new} = \begin{pmatrix} 1 & 1 \\ 0 & 1 \end{pmatrix}^{-1} \mathbf{w}_{\rm i} = \begin{pmatrix} 1 & -1 \\ 0 & 1 \end{pmatrix} \mathbf{w}_{\rm i} \tag{19b}$$

The above results are proven in various ways in a number of mathematical articles [8,9,15,29,10]. In the next section we explain how these properties of angle and action variables of the tori associated with H_0 lead to the dynamical behavior of the perturbed time-dependent system that was displayed in Fig. 3.

4. Dynamical monodromy

All of the discussion above in Section 3 deals with 'static' connections (continuous mappings of local angle variables) on a bundle of Liouville tori of the system with the time-independent Hamiltonian $H_0(\mathbf{q},\mathbf{p})$ in (2). What are the implications of this 'static' monodromy for the dynamical behavior of the system? We observed in the calculations (Fig. 3 and Result 1) that the initial loop is equivalent to $\gamma_2(0)$, and that the final loop is homotopic to $\gamma_2(0) - \gamma_1$; Eq. (14) indicates that this latter loop is $\gamma_2(60)$. More generally, we will see that the loop generated dynamically by our chosen perturbing vector field X_1 follows a smoothly evolving loop of the static system $\gamma_2(t)$ at all t.

To explain this, we now allow the static system to be perturbed by an additional vector field X_1 in (6). After a brief review of the dynamics of the unperturbed system in Section 4.1 (which is later extended in Section 4.3.2), we consider in Section 4.2 certain general requirements on *admissible* perturbations X_1, and then we define a particular perturbation which we use later in calculations and which we call *ideal*. We then choose an ensemble of trajectories, which we may imagine to be a collection of noninteracting particles, and follow the evolution of this ensemble under a perturbed flow φ^t. *This idea of observing an ensemble of particles is central to our approach.* By following the ensemble through time,

we find several distinct but closely related dynamical manifestations of the monodromy of the static system with Hamiltonian $H_0(\mathbf{q},\mathbf{p})$.

4.1. Unperturbed motion

4.1.1. Pericenter and reference orbit

A typical path of the particle between bounces is shown in Fig. 1. The point of this trajectory where both $|\mathbf{q}|$ and $|\mathbf{p}|$ attain their respective smallest possible values $\rho_{\min}$ and $p_{\min}$ (for given m and E) is called the *pericenter*. Notice that unless $m=0$ and $E>0$ (on the positive-E semiaxis) the pericenter is a turning point of the radial motion. (It is a 'fly through' point if $m=0$ and $E>0$.) Assuming $\mu=a=1$ [2], we obtain

$$\rho_{\min}=\sqrt{|E+\mathrm{i}m|-E} \tag{20a}$$

$$p_{\min}=\sqrt{|E+\mathrm{i}m|+E} \tag{20b}$$

for given m and E, see Fig. 1, left.

For each (m,E), we define a *reference orbit* on the torus $\Lambda_{(m,E)}$ as follows. The reference orbit extends from one bounce off the outer wall to the next one and either (i) if $m=0$ and $E<0$ it remains always in the plane $\{y=p_y=0\}$ or (ii) in all other cases it crosses the hyperplane $\{y=0\}\subset\mathbb{R}^4$ at $t=0$ at its pericenter. The latter is defined as the four vector

$$\mathbf{u}_0(m,E)=(x_0(m,E),0,0,p_0(m,E))^T \tag{21}$$

where x_0 and p_0 satisfy

$$x_0p_0=m \quad\text{and}\quad p_0^2-x_0^2=2E$$

so that $|x_0|=\rho_{\min}$ and $|p_0|=p_{\min}$. The signs of x_0 and p_0 will be chosen later (see Section 4.1.4). Defining the linear flow of the system with Hamiltonian H_0 by the 4×4 matrix

$$S^t_{H_0}=\begin{pmatrix}\cosh t & 0 & \sinh t & 0\\ 0 & \cosh t & 0 & \sinh t\\ \sinh t & 0 & \cosh t & 0\\ 0 & \sinh t & 0 & \cosh t\end{pmatrix} \tag{22}$$

the reference orbit is

$$\left[-\frac{1}{2},+\frac{1}{2}\right]\to\mathbb{R}^4:\xi\mapsto S^{\xi\tau}_{H_0}\mathbf{u}_0(m,E) \tag{23}$$

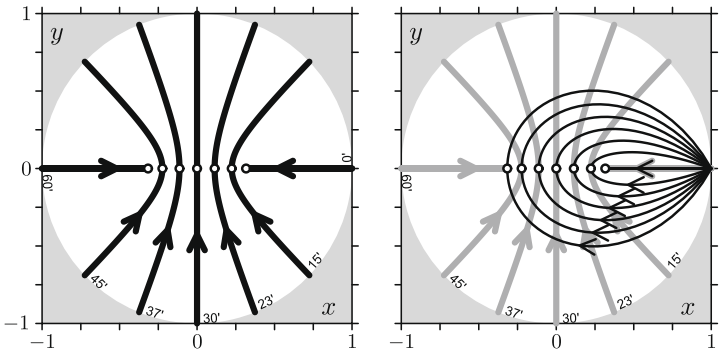

Fig. 5. Left: The (x,y)-trace of a family of reference orbits (bold) with (m,E) following the monodromy circuit Γ in Fig. 2; empty circles mark pericenters. Right: The (x,y)-trace of a family of cycles γ_2 (black) obtained from the respective reference orbits (gray). Axes x and y are scaled in units of $\rho_{\max}=\sqrt{2}$; $\mu=a=1$.

where $\tau = \tau(m,E)$ is computed in the next section and $\xi = \pm\frac{1}{2}$ represent points on the wall, see Figs. 1 and 5, left.

4.1.2. Period of first return and rotation angle

The time $\tau(m,E)$ between the bounces of the unperturbed motion under H_0 is called the *period of first return*. It is a single-valued smooth function $\mathbb{R}^2 \setminus 0 \to \mathbb{R}$ with a logarithmic singularity at the origin of the (m,E) plane,

$$\tau(m,E) = \cosh^{-1}\frac{\rho_{\max}^2 + E}{s} \tag{24a}$$

with

$$s(m,E) := |\mathbf{s}(m,E)| = |E + \mathrm{i}m| = \sqrt{E^2 + m^2} \geqslant 0$$

Near the origin when $0 < s(m,E) \ll \frac{1}{2}\rho_{\max}^2$

$$\tau(m,E) \approx \log 2\rho_{\max}^2 - \log|E + \mathrm{i}m| + \cdots \tag{24b}$$

The polar angle $\theta(m,E)$ swept in the $\mathbf{q}$-plane during $\tau(m,E)$ (Fig. 1) is called the *rotation angle* and is a multivalued function

$$\theta(m,E) = 2\tan^{-1}\left(\frac{E+s}{m}\sqrt{\frac{\rho_{\max}^2 + E - s}{\rho_{\max}^2 + E + s}}\right) \tag{25a}$$

which for $0 < s(m,E) \ll \frac{1}{2}\rho_{\max}^2$ has an asymptotic form

$$\theta(m,E) \approx \pi - \arg(E + \mathrm{i}m) + \cdots \tag{25b}$$

These quantities are central to the construction of the second action variable and to the analysis of 'static' monodromy.

For the monodromy circuit Γ in (7), we verify that $\tau \circ \Gamma$ and $\theta \circ \Gamma$ are smooth functions of parameter t illustrated in Fig. 6. Furthermore, from (24b) and (25b) we obtain

$$\tau(\mathbf{s}(t)) \approx \log 2\rho_{\max}^2, \quad \theta(\mathbf{s}(t)) \approx \Omega t, \qquad \mathbf{s}(t) \in \Gamma \tag{26}$$

To assess these asymptotic expressions note that for physical parameters in (3), the circuit Γ in (7) lies well inside the domain of regular $\mathcal{EM}$-values while encircling closely the critical value $\mathbf{s} = 0$, as shown Fig. 2, left. As a consequence, the simple approximations in (26) are quite accurate, see Fig. 6, left.

4.1.3. Tracing integral curves for arbitrary time

When the particle bounces off the wall at $\rho = \rho_{\max}$, the radial component p_ρ of its momentum $\mathbf{p}$ changes sign, while the polar component and the angular momentum are conserved. So it can be seen

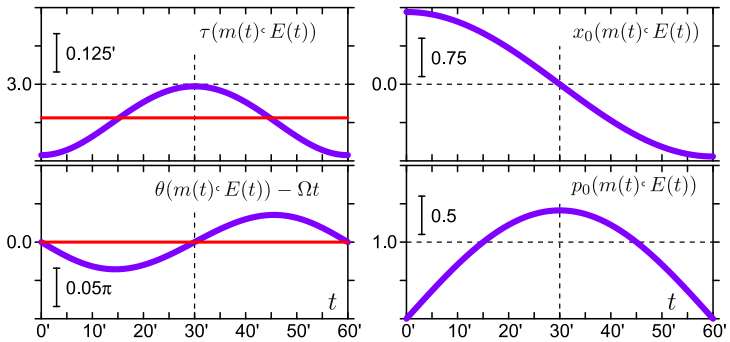

Fig. 6. Variation of the period of first return τ, the rotation angle θ, and the pericenter position (q_0, p_0) in (27) along the monodromy circuit Γ in (7) and Fig. 2.

that after the kth bounce, with $k = 1, 2, 3, \ldots$, the trajectory begins with the same initial conditions except for the polar angle ϕ advanced by $k\theta(m, E)$. Therefore, an (x, y) image of the complete trajectory can be constructed by projecting the phase curve followed for one period $\tau(m, E)$ and then repeating the resulting curve by rotating it by angle $k\theta(m, E)$ about the origin, see Fig. 1, right.

4.1.4. Continuous parameterization of integral curves

For the purposes of our further study, we should be able to parametrize integral curves of the system with Hamiltonian H_0 in (2) on each fiber $\Lambda_{(m,E)}$ by the values (m, E) and two additional dimensionless angle-like parameters. As $\mathbf{s} = (m, E)$ follows a continuous path in the (m, E)-plane, such as any open segment of the monodromy circuit Γ in Fig. 2, the corresponding parametric family of integral curves should be continuous.

We first define using (23) a continuous family of reference orbits for different (m, E). To this end we define appropriately the signs of the components x_0 and p_0 of $\mathbf{u}_0$ in (21): when passing through $\{m = 0, E > 0\}$ we change the sign of x_0, when passing through $\{m = 0, E < 0\}$ we change the sign of p_0. This makes $\mathbf{u}_0(m, E)$ smooth everywhere. For a single tour on monodromy circuit Γ in (7), i.e., for $t = [0, 60]$, it is sufficient to take

$$p_0 = p_{\min}(m, E) \geqslant 0 \tag{27a}$$

$$x_0 = \operatorname{sign}(m)\rho_{\min}(m, E), \quad \text{for } m \neq 0 \tag{27b}$$

$$x_0 = \pm\rho_{\min}(m, E), \quad \text{for } m = 0 \tag{27c}$$

From these equations and (7), we obtain

$$x_0(\mathbf{s}(t)) = \cos\frac{1}{2}\Omega t \quad \text{and} \quad p_0(\mathbf{s}(t)) = \sin\frac{1}{2}\Omega t \tag{27d}$$

as smooth functions of parameter t, see Fig. 6, right [33]. The resulting family of reference orbits is illustrated in Fig. 5, left. The exceptional reference orbits with $m = 0$ and $E < 0$ are *closed* at the wall [23]; all other reference orbits are open.

To parametrize all other orbits of the flow of the unperturbed system with Hamiltonian H_0, we use two phases t_0 and ϕ_0 in order to move the initial conditions $\mathbf{u}_0(m, E)$ to a different point on the torus $\Lambda_{(m,E)}$. Using $t_0 \in \left[-\frac{1}{2}\tau, \frac{1}{2}\tau\right]$ we shift along the reference orbit, and using ϕ_0 we move this orbit along the $\mathbb{S}^1$ orbits of the flow of the system with Hamiltonian M, i.e., we rotate it in $\mathbb{R}^4$ by matrix

$$S_M^{\phi} = \begin{pmatrix} \cos\phi & -\sin\phi & 0 & 0 \\ \sin\phi & \cos\phi & 0 & 0 \\ 0 & 0 & \cos\phi & -\sin\phi \\ 0 & 0 & \sin\phi & \cos\phi \end{pmatrix} \tag{28}$$

with $\phi = \phi_0$. So the general orbit is given by

$$\mathbf{u}(t) = S_{H_0}^{t-t_0} S_M^{\phi_0} \mathbf{u}_0(m, E) \tag{29}$$

Since the respective first integrals are in involution, $S_{H_0}^t$ and S_M^{ϕ} commute. Furthermore we note that initial conditions of the integral curve in (29) are given by four parameters (t_0, ϕ_0) and (m, E) so that all dependency on (m, E) is contained in the pericenter position $\mathbf{u}_0(m, E)$.

4.1.5. Continuous choice of cycles

Each regular torus $\Lambda_{(m,E)}$ [23] has two fundamental directed loops γ_1 and γ_2 which represent basis cycles $[\gamma_1]$ and $[\gamma_2]$ [34]. The loops γ_1 can be uniformly chosen on *all* $\Lambda_{(m,E)}$ as orbits of the action of the axial symmetry SO(2) induced in $\mathbb{R}^4$ by the Hamiltonian flow of angular momentum M. Projected on the (x, y) plane, γ_1 become circles of constant ρ, which are directed counterclockwise by X_M. Let us call them *ϕ-loops*.

The loop γ_2 can be constructed using reference orbits in (23), and we can define a continuous family $t \mapsto \gamma_2(t)$ with $t \in [0, 60]$ using the continuous family of reference orbits defined by (27). As $\gamma_2(0)$ we can take the respective exceptional reference orbit.

The family of cycles $[\gamma_2(t)]$ is obtained by combining the flow of the vector field X_M of momentum M, together with the vector field X_{H_0} of the unperturbed Hamiltonian H_0,

$$(\mathbf{q}(\xi),\mathbf{p}(\xi))^T = S_M^{-\xi\theta} S_{H_0}^{\xi\tau}(x_0,0,0,p_0)^T \tag{30a}$$

with (x_0,p_0) defined in (27) and

$$\xi \in \left[-\frac{1}{2},\frac{1}{2}\right] \tag{30b}$$

a dimensionless variable along the orbit. (If t is the time of the flow of the system with Hamiltonian H_0, then $\xi = t/\tau$.) By this construction, the resulting closed curve $\gamma_2 \subset \mathbb{R}^4$ is the orbit of the flow which is defined on the regular fibers $\Lambda_{(m,E)}$ of our system by the vector field X_{J_2} of the local action J_2, and ξ corresponds to the canonical angle variable w_2 [35]. For $\mathbf{s}(t) = (m(t),E(t))$ in any open segment of Γ in Fig. 2, for example if $0' < t < 60'$, the resulting curves

$$\gamma_2(t) : \left[-\frac{1}{2},\frac{1}{2}\right] \to \Lambda_{(m(t),E(t))} \subset \mathbb{R}^4 : \xi \mapsto (\mathbf{q}(\xi),\mathbf{p}(\xi))^T$$

form a continuous family of curves in $\mathbb{R}^4$ parameterized by one parameter t. This can be verified explicitly for Γ in (7) using (26) and (27d).

Projections of the resulting family of curves $\gamma_2(t)$ on the $\mathbf{q}$ plane $\mathbb{R}^2_{x,y}$ are shown in Fig. 5. We can see from this figure that $\gamma_2(0)$ projects to a radial segment of axis x with $0 < \rho_{\min} \leqslant \rho \leqslant \rho_{\max}$, while all other projections are directed $\mathbb{S}^1$ loops in $\mathbb{R}^2_{x,y}$ with one singular point or "tip" at the apocenter $\mathbf{q} = \rho_{\max}$. The loops are symmetric with respect to the radial line passing through their tips. Furthermore, the distance between the tip and the pericenter (empty circles in Fig. 5) increases monotonically with $t \in [0,60]$. So in particular, all projections of $\gamma_2(t)$ with $t > 30$ encircle the origin $\mathbf{q} = 0$ in $\mathbb{R}^2_{x,y}$.

These orbits γ_2 in Fig. 5, right, represent the second basis cycle $[\gamma_2]$ of the first homology of $\Lambda_{(m,E)}$. Since, as was already mentioned, the orbit $\gamma_2(0)$ (for $m = 0$ and $E < 0$) projects as a segment $[\rho_{\min},\rho_{\max}]$ of the positive semiaxis x in the $\mathbf{q}$-plane, we can call $\gamma_2(0)$ a *radial orbit* or *ρ-loop*; for all other γ_2 orbits such terminology is misleading.

The cycle bases $\{[\gamma_1],[\gamma_2]\}$ form a continuous bundle of first homologies H_1 [36] over the circuit $\Gamma \sim \mathbb{S}^1$ in Fig. 2. This bundle is locally trivial, but [since the static system with Hamiltonian H_0 has monodromy and Γ goes around the isolated critical $\mathcal{EM}$-value $(0,0)$ and is therefore not homotopic to 0] it is globally nontrivial. Specifically, while the globally defined cycle γ_1 remains unchanged,

$$\gamma_1(60) = \gamma_1(0) \tag{31a}$$

the initial cycle $\gamma_2(0)$ and the final cycle $\gamma_2(60)$ are related by (14),

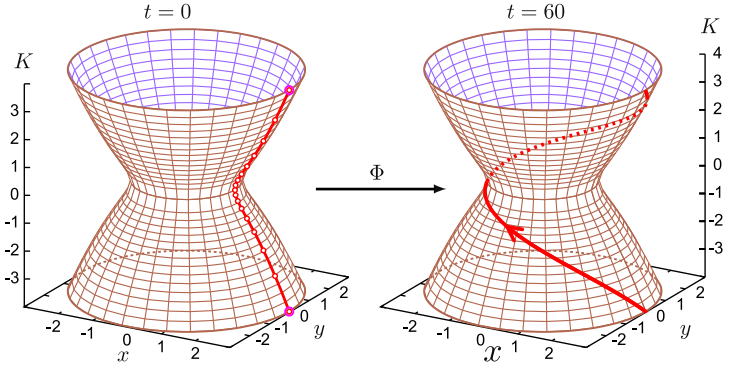

Fig. 7. Initial and final cycles $\gamma_2(0)$ and $\gamma_2(60)$ defined by (30), (7), and (26) on the torus $\Lambda_{(m,E)}$ with $(m,E) = (0,-1)$ immersed in $\mathbb{R}^3$ with coordinates x,y, and $K = \frac{1}{2}(xp_x + yp_y)$.

$$\gamma_2(60) = \gamma_2(0) - \gamma_1(0) \tag{31b}$$

To see the latter, note that for any $(m, E > E_{\min}(m))$, i.e., for any allowed $\mathcal{EM}$-value in the shaded domain in Fig. 2 (left), and any t, an orbit γ_1 projects to a circle in the $\mathbf{q}$-plane which goes counterclockwise and parallel to the wall, while $\gamma_2(60)$ is directed clockwise and intersects the wall at one point as shown in Fig. 5. Finally, the three-dimensional representation of the initial–final torus $\Lambda_{(m,E)}$ [37] in Fig. 7 can also help to understand better the relation of $\gamma_2(0)$ and $\gamma_2(60)$. This representation clearly shows that the two cycles are not homotopic to each other.

4.1.6. Description of motion on tori

The coordinates on regular tori $\Lambda_{(m,E)}$ [23] in $\mathbb{R}^4$ are defined by values $\mathbf{w}$ of local angle variables $\mathbf{W} = (W_1, W_2)$ [5] which give Liouville lengths along the basis cycle representatives γ_1 and γ_2 of $\Lambda_{(m,E)}$. The origin $\mathbf{w} = 0$ of the coordinates can be fixed uniformly using $\mathbf{u}_0(m, E)$.

Under the unperturbed flow of $X_{H_0} = X_0$, the angles $\mathbf{w}(t)$ evolve linearly with time according to (8) as illustrated in Fig. 8. The frequencies of this motion are

$$\boldsymbol{\nu}(m, E) = (\nu_1, \nu_2) = \left(\frac{\theta(m, E)}{\tau(m, E)}, \frac{2\pi}{\tau(m, E)}\right)\frac{1}{2\pi} \tag{32}$$

Note that $\nu_2 = 1/\tau$ is the frequency of the radial motion.

4.2. Choosing admissible perturbing terms

In the perturbed system with full flow φ^t given by the vector field X in (6), there are many concrete ways to accomplish changes in the values of angular momentum m and energy E, which are defined to be the instantaneous values of M in (4) and H_0 in (2). We begin with certain simple general requirements for *admissible* perturbing vector fields X_1 in (6) which can be used to exhibit monodromy dynamically.

Let $\mathbf{s}$ denote points (values of the $\mathcal{EM}$ map) in the image of the $\mathcal{EM}$ map in $\mathbb{R}^2$ with coordinates (m, E). As before (Fig. 2), the monodromy circuit Γ is a closed directed path going around the monodromy center $\mathbf{s} = (0, 0)$; both Γ and its sufficiently small open neighborhood R_Γ consist of regular $\mathcal{EM}$ values. The preimage (the fiber) $\mathcal{EM}^{-1}\mathbf{s}$ of any regular $\mathcal{EM}$ value $\mathbf{s}$ is a single regular torus $\Lambda_\mathbf{s}$ [23]. For points $\mathbf{s}$ on Γ, we consider their small open regular neighborhoods $\sigma_\mathbf{s} \subseteq R_\Gamma$ containing regular $\mathcal{EM}$ values $\mathbf{s}', \mathbf{s}''$, etc. We also consider the corresponding small open neighborhoods $\Sigma_\mathbf{s} = \mathcal{EM}^{-1}\sigma_\mathbf{s}$ of regular tori $\Lambda_\mathbf{s}$ containing regular tori $\Lambda_{\mathbf{s}'}, \Lambda_{\mathbf{s}''}$, etc. Finally, we consider trajectories in the extended phase space $\mathbb{R}^4 \otimes \mathbb{R}^1$ with coordinates $((\mathbf{q}, \mathbf{p}), t)$ evolving under the flow φ^t, and we describe how these trajectories evolve through the extended subspaces $(\Lambda_\mathbf{s}, t), (\mathcal{EM}^{-1}(\sigma_\mathbf{s}), t)$, etc.

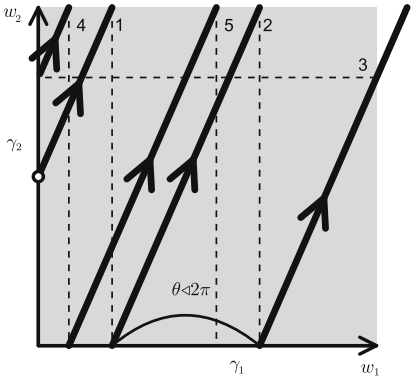

Fig. 8. Trajectory of the flow of the unperturbed system (bold black) on the regular fiber $\Lambda_{(m,E)}$ with local angle coordinates (w_1, w_2); empty circle marks $t = 0$, numbers refer to consecutive segments.

(1) An admissible perturbing vector field $X_1(\mathbf{q},\mathbf{p})$ acts during the time t in $(t_i,t_f)\subset\mathbb{R}$ with $-\infty<t_i<t_f<\infty$ and vanishes for times outside this interval. The resulting admissible full flow φ^t defines a continuous mapping, and furthermore, for all $(\mathbf{q},\mathbf{p})$ in $\mathcal{EM}^{-1}(R_\Gamma)\setminus\{q=\rho_{\max}\}$ this mapping is piecewise smooth in t and locally smooth in $(\mathbf{q},\mathbf{p})$.
(2) Under the flow φ^t, the trajectories starting in $\mathcal{EM}^{-1}(R_\Gamma)$ are continuous (except for the bounces at $\rho=\rho_{\max}$ [23]) and are nonintersecting curves in $\mathbb{R}^4\otimes\mathbb{R}^1$ which depend continuously on the initial conditions.
(3) In order to make E and/or m evolve, X_1 should be transversal to regular tori $\Lambda_{\mathbf{s}}$, i.e., to both vector fields X_{H_0} and X_M. We will assume for simplicity that this holds at all times in (t_i,t_f) for all $\mathbf{s}$ in $R_\Gamma\supset\Gamma$.
(4) Under $\varphi^t(\mathbf{q},\mathbf{p})$, any $\mathbf{s}'(t)$ starting at $t=t_i$ in a neighborhood $\sigma_{\mathbf{s}_i}$ of $\mathbf{s}_i=\mathbf{s}(t_i)\in\Gamma$, evolves continuously (and piecewise smoothly) through R_Γ so that $\mathbf{s}'(t)=(s'_m(t),s'_E(t))\in\sigma_{\mathbf{s}(t)}$ of some $\mathbf{s}(t)\in\Gamma$ that traverses Γ continuously and counterclockwise, and comes back to $\mathbf{s}_f=\mathbf{s}(t_f)=\mathbf{s}_i$ at time $t=t_f$.
Two consequences of the above conditions follow.
(5) Points $\mathbf{s}'(t_i)$ and $\mathbf{s}'(t_f)$ lie in the same small open neighborhood $\sigma_{\mathbf{s}_i}=\sigma_{\mathbf{s}_f}$. So connecting $\mathbf{s}'(t_f)$ and $\mathbf{s}'(t_i)$ inside that neighborhood, we obtain a closed curve $\Gamma'\subset R_\Gamma$ homotopic to Γ.
(6) Under $\varphi^t(\mathbf{q},\mathbf{p})$, a loop $\gamma_i\subset\Sigma_{\mathbf{s}_i}$ evolves continuously in $\mathbb{R}^4\otimes\mathbb{R}^1$ so that $\gamma(t)=\varphi^t(\gamma_i)\subset\Sigma_{\mathbf{s}(t)}$ remains a loop that returns to $\Sigma_{\mathbf{s}_i}$ at $t=t_f$. In $\Sigma_{\mathbf{s}_i}$, this defines a bijective map $\gamma_i\to\gamma_f$. At the same time, the image $\mathcal{EM}(\gamma(t))\subset\sigma_{\mathbf{s}(t)}$ of $\gamma(t)$ stays a connected set which comes back to $\sigma_{\mathbf{s}_i}$.

To have an example of an admissible perturbation, consider local angle–action variables $(\mathbf{J},\mathbf{W})$ of the unperturbed system (Section 4.1.6) which are well defined locally (smooth, real, and in case of local actions—single valued) functions of $(\mathbf{q},\mathbf{p})$. So rewriting X in (6) as

$$X(\mathbf{j},\mathbf{w},t)=X_0(\mathbf{j})+X_1(\mathbf{j},\mathbf{w},t) \tag{33a}$$

equations of motion for the values $(\mathbf{j},\mathbf{w})$ of $(\mathbf{J},\mathbf{W})$ are

$$\frac{d}{dt}\begin{pmatrix}\mathbf{j}\\ \mathbf{w}\end{pmatrix}=\begin{pmatrix}0\\ \boldsymbol{\nu}(\mathbf{j})\end{pmatrix}+X_1(\mathbf{j},\mathbf{w},t) \tag{33b}$$

with frequencies $\boldsymbol{\nu}$ from (8).

If we now restrict X_1 so that

$$X_1(\mathbf{j},\mathbf{w},t)=\begin{pmatrix}\mathbf{c}(t)\\ 0\end{pmatrix} \tag{34}$$

where functions $\mathbf{c}=(c_1,c_2)$ are piecewise smooth in t, then angles $\mathbf{w}$ evolve under the full flow φ^t just as they would evolve under the unperturbed φ_0^t in (8), i.e.,

$$d\mathbf{w}/dt=\boldsymbol{\nu}(\mathbf{j}) \tag{35}$$

The perturbing vector field X_1 in (34) and the resulting total flow φ^t will be called *ideal*. It has important special properties. Specifically, the rate of change of action values $\mathbf{j}(t)$ equals $\mathbf{c}(t)$ for any particle within the domain of definition of the local action–angle variables $(\mathbf{J},\mathbf{W})$. Hence (within this domain) particles will move synchronously from one torus to another so that if all particles begin at $t=t_i$ on one torus $\Lambda_{\mathbf{s}_i}$, then at every instant t they will all remain on a single torus $\Lambda_{\mathbf{s}(t)}$ [38]. Until Section 6, we will discuss only ideal flows φ^t. The following lemma follows.

Lemma 1. local evolution *Under the ideal flow φ^t defined locally in a sufficiently small open regular neighborhood $\Sigma_{\mathbf{s}_0}$ of a regular fiber $\Lambda_{\mathbf{s}_0}$, the values $\mathbf{j}=\mathbf{j}(t)$ of local actions can be made to vary so that the energy–momentum values $\mathbf{s}(\mathbf{j}(t))\in\sigma_{\mathbf{s}_0}$ follow a portion $\delta\Gamma_{\mathbf{s}_0}=\sigma_{\mathbf{s}_0}\cap\Gamma$ of the path Γ. At the same time, the evolution of local angles $\mathbf{w}$ is obtained by integrating $\boldsymbol{\nu}(\mathbf{j}(t))$. Specifically*

$$w_1(t)=\frac{1}{2\pi}\int_0^t\frac{\theta(m(t),E(t))}{\tau(m(t),E(t))}\,dt+w_1(0)$$

$$w_2(t) = \int_0^t \frac{1}{\tau(m(t), E(t))}\, dt + w_2(0)$$

Furthermore the perturbation X_1 is well defined both as $X_1(\mathbf{q}, \mathbf{p}, t_0)$ and $X_1(\mathbf{j}, \mathbf{w}, t_0)$.

Indeed, by the theorem assuring the existence of local action–angle variables [3], the map

$$\sigma_{\mathbf{s}_0} \to \mathbb{R}^2 : \mathbf{s} \mapsto \mathbf{j}(\mathbf{s})$$

relating (the values of) energy–momentum and local actions is a local diffeomorphism. (Note that while $j_1 \equiv 2\pi m$, the locally single-valued function $j_2(m, E)$ is globally multivalued.) So the first statement of the lemma is obtained after choosing an appropriate $\mathbf{c}(t)$ in (34). By the same theorem, there is a diffeomorphism $(\mathbf{J}, \mathbf{W})$ relating the neighborhoods $\Sigma_{\mathbf{s}_0}$ in the $(\mathbf{q}, \mathbf{p})$-space and in the $(\mathbf{j}, \mathbf{w})$-space. Therefore X_1 is well defined in either space. The second statement follows from (35) and (32).

Lemma 1 gives us a tool to construct a perturbation which produces a desired change of m and E in a sufficiently small open neighborhood $\sigma_{\mathbf{s}}$ of any regular $\mathcal{EM}$-value $\mathbf{s} = (m, E)$, i.e., locally. What we really want is a perturbation that causes $\mathbf{s}(t)$ to traverse the whole monodromy circuit Γ. We call any concrete perturbation X_1 a *realization of the monodromy circuit* Γ if under such perturbation $\mathbf{s}(t)$ completes a tour on Γ.

Theorem 1. global realization). *Ideal realizations $X_1(\mathbf{q}, \mathbf{p}, t)$ or $X_1(\mathbf{j}, \mathbf{w}, t)$ of the monodromy circuit Γ exist. They are defined on $\mathcal{EM}^{-1}(R_\Gamma) \times [t_\mathrm{i}, t_\mathrm{f}]$ and are smooth in $(\mathbf{q}, \mathbf{p})$ or $(\mathbf{j}, \mathbf{w})$ and piecewise smooth in t.*

A constructive proof of Theorem 1 relies on Lemma 1. It can be sketched as follows. Consider intermediate times $t_\mathrm{i} = t_0 < t_1 < t_2 < \cdots < t_{N-1} < t_N = t_\mathrm{f}$ with N finite, which divide $[t_\mathrm{i}, t_\mathrm{f}]$ into adjacent segments $[t_k, t_{k+1}]$, and let $\mathbf{s}_k \in \Gamma$ be the (m, E)-value at time t_k. Let open overlapping neighborhoods $\sigma_{\mathbf{s}_k}$ cover Γ so that R_Γ is a union $\bigcup_{k=0}^{N} \sigma_{\mathbf{s}_k}$. Within the neighborhood $\Sigma_{\mathbf{s}_k} = \mathcal{EM}^{-1}\sigma_{\mathbf{s}_k}$ of any regular torus $\Lambda_{\mathbf{s}_k}$ we can use well defined local action–angle variables $(\mathbf{J}, \mathbf{W})^{(k)}$ [3] and therefore by Lemma 1 we can traverse the part $\Gamma \cap \sigma_{\mathbf{s}_k}$ of the monodromy circuit using an appropriately chosen perturbation $X_1^{(k)}$ in (34) during the time in $[t_k, t_{k+1}]$. This locally defined $X_1^{(k)}$ is a smooth function of $(\mathbf{j}, \mathbf{w}, t)$ and therefore of $(\mathbf{q}, \mathbf{p}, t)$. The local action–angles $(\mathbf{J}, \mathbf{W})^{(k)}$ defined in $\Sigma_{\mathbf{s}_k}$ can be redefined smoothly (or at least continuously) as we go along Γ by the choice of the specific smooth (or continuous) family of basis cycles $[\gamma_2]$ and the corresponding action J_2 and angle W_2. This will define local diffeomorphisms between $(\mathbf{J}, \mathbf{W})^{(k)}$ and $(\mathbf{J}, \mathbf{W})^{(k+1)}$, exploiting which in the overlap domains $\Sigma_{\mathbf{s}_k} \cap \Sigma_{\mathbf{s}_{k+1}}$ and the freedoms of the concrete choices of local action–angle variables, we can match the 'junction values' $X_1^{(k)}(\mathbf{j}, \mathbf{w}, t')$ and $X_1^{(k+1)}(\mathbf{j}, \mathbf{w}, t')$ for some $t' \in [t_k, t_{k+1}]$ and thus make X_1 (at least) continuous on $[t_\mathrm{i}, t_\mathrm{f}]$. Note that in principle to cover the whole of $\mathcal{EM}^{-1}(R_\Gamma)$, two neighborhoods Σ are sufficient, and likewise R_Γ can be covered by a union of two σ.

4.3. The main result: observing cycle change by tracking motion in space and time

At last we can explain the main result illustrated in Fig. 3. We ask now what physical phenomena will be observed when a realization X_1 in (6) and (34) of the monodromy circuit is set to work [using in our case the parameter values in (3)]. To this end, Lemma 1 and Theorem 1 together with the explicit construction of cycle γ_2 in Section 4.1.5 are sufficient. We construct the ideal realization X_1 of the monodromy circuit Γ in Fig. 2 parameterized by (7) so that $\mathbf{s}(t_\mathrm{i}) = \mathbf{s}(t_\mathrm{f}) = (0, -1)$ with $t_\mathrm{i} = 0$ and $t_\mathrm{f} = 60$.

We analyze the $\mathbf{q}$-space projections $t \mapsto (x(t), y(t))$ of the trajectories of the perturbed system which follow the vector field in (6). At the initial time 0, we begin with a continuous one-parameter family of particles which constitute a ρ-loop on the initial torus $\Lambda_{\mathbf{s}(0)}$. We let this family of trajectories evolve under our ideal time-dependent perturbation. What happens to the initial loop? We have our main Result 1 which is illustrated in Fig. 3. The particles start on the ρ-cycle $\gamma_2(0)$ and evolve locally according to Lemma 1; by Theorem 1, our explicit construction of the smooth family of cycles γ_2 (see Section 4.3.2) defines X_1 globally and allows us to take the particles around the whole of Γ.

4.3.1. Relation to monodromy

Result 1 is now the natural consequence of the ideal time-dependent perturbation X_1. Recall that the initial ρ-loop is both a particular closed orbit (exceptional reference orbit in Section 4.1.1) of the flow of the unperturbed system and also a representative of the cycle $\gamma_2(0)$ in the first homology group of $\Lambda_{\mathbf{s}(0)}$. Under X_1, particles stay on the loop $\gamma_2(t)$ which evolves smoothly so that at all times the curve $\gamma_2(t)$ belongs to fiber $\Lambda_{\mathbf{s}(t)}$ with $\mathbf{s}(t) = (m(t), E(t))$ which follows Γ as described by (7). Considering $\gamma_2(t)$ for $t \in [0 \ldots 60]$ gives, therefore, a *dynamical connection* on tori $\Lambda_{\mathbf{s}(t)}$ swept by our realization of the monodromy circuit. This fulfills the conditions of the monodromy theorem in Section 3.3. So the ϕ-cycle γ_1 is unchanged, while any ρ-loop $\gamma_2(0)$ evolves into a combination of a ρ-loop and a ϕ-loop specified in (31). We come to our Result 1 which is, therefore, a dynamical consequence, observable in real time, of the monodromy of the underlying unperturbed (or "static") system.

4.3.2. Details of computation of loop evolution

Under the ideal perturbation X_1 defined by the family of cycles γ_2 in (30), particle trajectories are computed as follows. In the phase space $\mathbb{R}^4$, our particles start on the ρ-loop $\gamma_2(0)$ for which the rotation angle $\theta(0)$ is 0. So at $t = 0$ the particles lie in the plane $\{y = p_y = 0\}$ and their initial position x and momentum p_x are parameterized by

$$\left[-\frac{1}{2}, +\frac{1}{2}\right] \to \mathbb{R}^4 : \xi \mapsto (\mathbf{q}(\xi), \mathbf{p}(\xi))^T = S_{H_0}^{\xi\tau}(x_0, 0, 0, 0)^T$$

where x_0 is the inner turning point of the initial loop on the initial torus. In the local angle coordinates $\mathbf{w} = (w_1, w_2)$, these initial conditions correspond to $w_1(0) = 0$ and $w_2(0) = \xi_{0,i}$ for particle $i = 1, 2, 3, \ldots$

By Lemma 1, local angles $\mathbf{w}$ evolve under $X_{H_0} + X_1$ just as they would evolve under X_{H_0}, i.e., according to linear Eq. (8) albeit with frequencies $\boldsymbol{\nu}(m, E)$ changing as (m, E) follows Γ and the particles go from torus to torus. Local action–angle variables define a local isomorphism of the tori which allows us to view the latter projected to a *single* abstract $\mathbb{Z}^2$ lattice whose basis cell is represented in Fig. 8. So we can observe the evolution of γ_2 in this cell, bearing in mind that at different times, the actual phase space image of γ_2 is different and is given by (30) where θ, τ, x_0 and p_0 in (25b), (24b), and (27) are functions of $(m, E) = (m(t), E(t))$ illustrated in Fig. 6.

In the coordinates $\mathbf{w} = (w_1, w_2)$, the flow of the ideal perturbation is linear. Two things happen: at all times t, all particles move along the curve γ_2 by the same amount $\Delta w_2(t)$, while γ_2 as a whole is translated parallel to axis w_1 by $\Delta w_1(t)$. The quantities Δw_1 and Δw_2 are given by the integrals in Lemma 1, and since $w_1(0) = 0$ we have $\Delta w_1(t) = w_1(t)$.

To compute the time evolution of the whole initial loop, we only need to compute the loop called $\gamma_2(t)$ as given in (30) and shown in Fig. 5, and then rotate it clockwise by the angle $\phi_1(t) = 2\pi\Delta w_1 = 2\pi w_1(t)$.

To find the instantaneous phase-space coordinates of a particular particle at time t, we define

$$\xi(t) = \mathrm{Mod}_1(\xi_0 + \Delta w_2(t))$$

where the function Mod_1 subtracts the necessary integer to place $\xi(t)$ in the interval $\left[-\frac{1}{2}, +\frac{1}{2}\right)$

$$\mathrm{Mod}_1 : \mathbb{R} \to \left[-\frac{1}{2}, +\frac{1}{2}\right) : x \mapsto x - \max\{n \in \mathbb{Z} \,|\, x + \frac{1}{2} \geqslant n\}$$

Then the phase space position of the particle that began with initial value of ξ equal to ξ_0 is

$$(\mathbf{q}(t), \mathbf{p}(t))^T = S_M^{\phi_1(t) - \xi(t)\theta} S_{H_0}^{\xi(t)\tau}(x_0(t), 0, 0, p_0(t))^T \tag{36}$$

where, as always, $x_0(t), p_0(t)$ satisfy (27).

The integrals in Lemma 1 can be pretty well approximated as

$$\phi_1 \approx \frac{1}{2} t^2 \Omega \tau^{-1} \quad \text{and} \quad \phi_2 \approx 2\pi(\xi_0 + t\tau^{-1}) \tag{37}$$

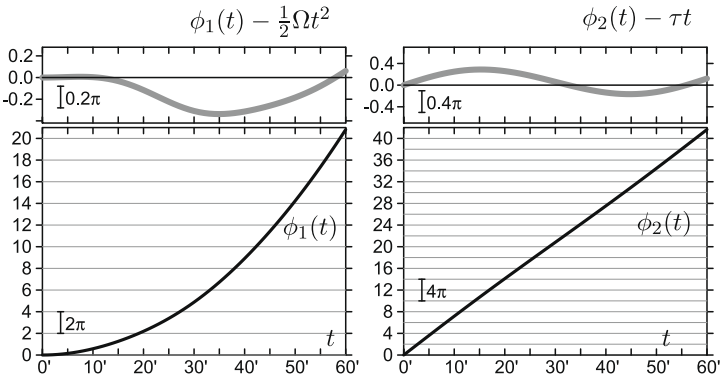

Fig. 9. Evolution of the local angle variables $\phi_1(t)$ (left) and $\phi_2(t)$ (right) under the ideal perturbation associated with the monodromy circuit Γ in (7) and Fig. 2 and the continuous family of cycles $[\gamma_2]$ in (30); top plots show the difference from the values based on asymptotic expressions in (24b) and (25b).

(see Fig. 9), but these approximations are not adequate for accurate computation of the location of the loop or of an individual particle. The snapshots in Fig. 3 are computed using numerically integrated exact expressions for $\theta(m,E)$ and $\tau(m,E)$.

In the consecutive snapshots in Fig. 3, where the current time t is indicated in the upper right corner of each fragment, the family of particles on γ_2 is followed using the approach detailed above. We display γ_2 (bold solid line) after equal intervals $\Delta t = 5'$. At $t > t_i = 0$ $\gamma_2(0)$, or the initial ρ-loop, becomes a loop $\mathbb{S}^1$ in the **q**-space with one singular point at which this loop is constantly 'attached' to the wall. These loops are rotated images of the curves γ_2 in Fig. 5, right, and at each particular time t, their singular point corresponds to a different particle bouncing off the wall. As time increases and individual particles move around and bounce off the wall, the loop as a whole can be obtained by interpolating between the instantaneous **q**-space positions of adjacent particles. We can see that this loop 'inflates' and its singular point moves counterclockwise for $t = 0' \ldots 30'$, i.e., until we reach $m = 0$ and $E = 1$ (cf. Figs. 2 and 3). During this period, the radius of the classically forbidden region in configuration space shrinks, so that at $t = 30$, when $m(t) = 0$ and $E(t) > 0$, the region vanishes. At that very instant, one point of the loop 'slips' through $\mathbf{q} = 0$ and moves to the 'other side'. Because the loop remains continuous, this point "carries the loop with it". We can see in Fig. 3 that the loop reaches, and an instant later—embraces $\mathbf{q} = 0$. Then as $m(t)$ becomes negative, the classically forbidden region continuously grows again, but this time *inside* the loop. Meanwhile, the individual particles on the loop begin moving clockwise; on the other hand, the tip of the loop continues moving counterclockwise at an increasing rate, while the loop as a whole continues inflating ever further. When we stop the movie on $(\Lambda_{(0,-1)}, t_f = 60)$, we see a loop that starts at the wall, goes clockwise once around $(x,y) = 0$ and closes back at the wall.

5. Further manifestations of dynamical monodromy

Result 1 is of a topological nature and as such it remains valid for a large class of admissible realizations of the monodromy circuit, for other initial conditions etc. In this section we consider other possibilities to observe dynamical monodromy (Results 2 and 3) which are more sensitive to the realization of the monodromy circuit.

5.1. Observing changes of angle variables

We now consider the motion of individual members of the family of particles considered previously. To this end we study the evolution of the value $w_2(t)$ of the second angle variable which determines the instantaneous position $\xi(t)$ of the particle on $\gamma_2(t)$, cf. Eq. (36). In Fig. 3 we traced the path of the particle which started at the wall ($x(0) = \rho_{max}$ and $\xi(0) = \pm\frac{1}{2}$). In each snapshot, the most recent

part of the trajectory during the time in $(t-\Delta t, t)$ is highlighted by a bolder line beginning at the endpoint of the preceding fragment.

Our particle first oscillates along the x-axis ($t = 0 \ldots 5'$ in Fig. 3). As its angular momentum m and energy E increase ($t = 5' \ldots 15'$), it begins moving around counterclockwise in ever larger leaps between subsequent bounces against the wall. When E goes towards its maximum value 1 and m drops back to 0 ($t = 15' \ldots 30'$), the leaps of the particle keep increasing and become nearly π so that the particle moves on nearly a straight line close to the origin. After m becomes negative ($t = 30' \ldots 45'$), the particle begins bouncing *clockwise* in decreasing leaps. And finally, as E goes down back to -1 and m increases to 0, it ends up again bouncing along a radial line. Other particles have similar trajectories.

The final azimuthal angle $\phi_f = \phi(60)$ of the particle depends on its initial azimuthal angle $\phi_i = \phi(0) = 0$ and on the rate of change of ϕ along the trajectory. It can be computed using (36) for $t = 60$ [note that $\phi(0) = \phi_1(0)$ and $\theta(60) = 2\pi$]. Suppose we start two particles, I as described above and II with the same $\rho(0) = \rho_{max}$ and $\mathbf{s}(0)$, but at a different initial angle $\phi_{II}(0) \neq 0$. Due to the axial symmetry, the trajectory of II is just a rotation of that of I, and the angle difference remains always unchanged:

$$\Delta\phi_f = \phi_{II}(60) - \phi_I(60) = \phi_{II}(0) - \phi_I(0) = \Delta\phi_i$$

Now suppose instead that particle II starts at the *same* azimuthal angle $\phi_{II}(0) = 0$, i.e., both particles start on $\gamma_2(0)$ with $y(0) = 0$, but with $x_{II}(0) = \rho_{min}$, i.e., at the inner turning point or pericenter with $\xi = 0$, half a ρ-cycle away from particle I. In Fig. 3, the trajectory of this particle is not shown but its position on $\gamma_2(t)$ is indicated along with the position of particle I. Averaging $d\phi/dt$ over each leap of the particles, we may expect naively that their trajectories would subtend nearly the same total azimuthal angle, and we may expect to find a small $\Delta\phi_f$. This turns out to be not true; instead we arrive at

Result 2. For ideal realizations of the monodromy circuit Γ, similar to the one illustrated in Figs. 2 and 3,

$$\Delta\phi_i = 0 \quad \text{and} \quad \Delta\phi_f = \phi_{II}(60) - \phi_I(60) = \pm\pi \tag{38}$$

For many admissible realizations, $\Delta\phi_f$ deviates substantially from $\Delta\phi_i = 0$ and is close to $\pm\pi$.

Thus in Fig. 3, particles I and II started on the torus with $\mathbf{s} = (0, -1)$, at the same polar (azimuthal) angle ϕ, and precisely half-cycle apart in their ρ motion. After an *ideal* realization of the monodromy circuit, they were still a half-cycle apart in their ρ motion, but they were also half a circle apart in ϕ.

With the knowledge of the system that we have acquired already, Result 2 can be explained easily. The angle variables $\mathbf{w}$ evolve linearly and at the same rate for each particle. This means that for any $t = 0 \ldots 60$

$$\Delta\xi(t) = w_{2,II}(t) - w_{2,I}(t) = \mp\frac{1}{2}$$

with the sign $\mp$ depending on whether we consider the particle I at the outer wall started with $\xi = w_2 = +\frac{1}{2}$ (before impact) or $-\frac{1}{2}$ (after impact). In particular, the particles are a half-cycle apart on $\gamma_2(60)$. [The latter is defined by Eq. (36) and is the loop defined by (30) rotated by $2\pi\Delta w_1(60)$.] Then by (31b), the final particles should be a half-cycle apart on the ρ-cycle $\gamma_2(0)$ *and* a half-cycle apart on the minus ϕ-cycle $-\gamma_1(0) = -\gamma_1$. More formally, at $t = 0$ we have

$$\Delta\mathbf{w}(0) = \mathbf{w}_{II}(0) - \mathbf{w}_I(0) = \left(0, \mp\frac{1}{2}\right) \tag{39}$$

Upon return to the original torus at $t = 60$, the angle variables $\mathbf{W}$ have changed according to (18), and so, applying Eq. (19b), the distance between the new points, to which the particles return, is defined in the old coordinates as

$$\Delta\mathbf{w}(60) = \mathbf{w}_{II,new} - \mathbf{w}_{I,new} = \left(\pm\frac{1}{2}, \mp\frac{1}{2}\right) \tag{40}$$

Since for $m = 0$ and $E < 0$, the value w_1 of the canonical angle W_1 times 2π equals the polar angle ϕ representing the location of the particle, we get immediately that our particles arrive $\pm\pi$ apart in ϕ.

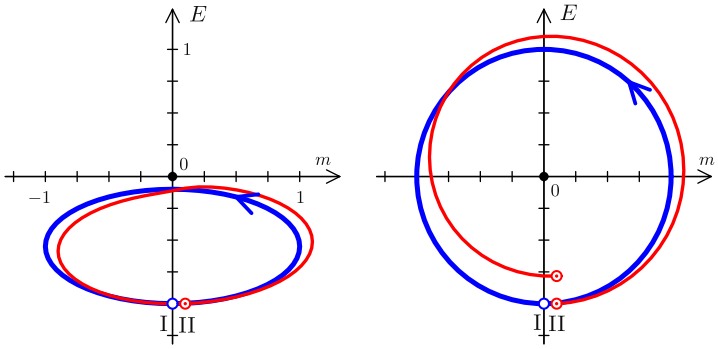

Fig. 10. Evolution of particles I (bold solid line) and II (fine solid line) starting at $t = t_i = 0$ with the same energy $E(t_i) = -1$ and slightly different angular momenta $m_I(t_i) = 0$ and $m_{II}(t_i) = \delta_m = 0.1$ along the placebo circuit (left) and monodromy circuit $\Gamma = \{|E + im| = 1\}$ (right) for the system with parameters in (3); both plots have the same $\mathcal{EM}$ scale as in Fig. 2, right.

5.2. Tracking motion in time and energy and observing changes of action variables

We consider now our monodromy circuit Γ along with a placebo circuit mentioned in Section 3.3 and let $(0, E(0))$ with $E(0) < 0$ be the initial–final point of both circuits (see Fig. 2). We take the ideal realization of the monodromy circuit Γ with perturbing vector field X_1^Γ that we used previously, and an ideal perturbation X_1^{placebo} which makes (m, E) traverse the placebo circuit (by Theorem 1). At $t = t_i = 0$, we place particles I and II at neighboring initial regular tori $\Lambda_i^{(I)}$ and $\Lambda_i^{(II)}$ with the same energy $E(0) = E_i < 0$ but slightly different momenta $m_{I,i} = 0$ and $m_{II,i} = \delta_m$. We let the system evolve under X_1^Γ or X_1^{placebo} until the 'reference' particle I comes back to $\Lambda_f^{(I)} = \Lambda_i^{(I)} = \Lambda_{0,E_i}$ at time $t = t_f = 60$. For δ_m sufficiently small, the energy–momentum of particle II will follow nearly the same circuit as particle I (see Fig. 10). What are the final energy–momentum of particle II? We observe

Result 3. Under any ideal X_1^{placebo}, particle II comes back to its initial torus $\Lambda_i^{(II)}$. However for any ideal X_1^Γ, it does not come back to its original torus $\Lambda_i^{(II)}$, but to a torus $\Lambda_f^{(II)}$ with the same original momentum $m_{II,f} = m_{II,i} = \delta_m$ but with energy $E_{II,f}$ shifted by $(2\pi/\tau)\delta_m$, where $\tau > 0$ is the period of first return of the flow of X_{H_0} on the torus $\Lambda_i^{(I)}$.

To understand Result 3, consider actions J_k as functions $\mathcal{J}_k(m, E)$ [7] which define the map

$$\mathcal{J} = (\mathcal{J}_1, \mathcal{J}_2) : D^* \to \mathbb{R}^2 : (m, E) \mapsto (2\pi m, j_2) = \mathbf{j}$$

on the set D^* of regular $\mathcal{EM}$-values. (D^* is a disk $D \ni 0$ punctured at 0.) As the energy and momentum of the particles evolve smoothly with time following a smooth circuit, the values of $\mathcal{J}(m, E)$ should also change smoothly.

In a sufficiently small regular neighborhood $\sigma_{\mathbf{s}} \subset D^*$ of any $\mathbf{s}$ in D^*, the map $\mathcal{J}$ is a diffeomorphism with linearization

$$\mathcal{J}(m + dm, E + dE) \approx \mathcal{J}(\mathbf{s}) + D\mathcal{J}(\mathbf{s}) \begin{pmatrix} dm \\ dE \end{pmatrix}$$

where the Jacobian matrix [see Section 3.3 and Eq. (16)]

$$D\mathcal{J}(\mathbf{s}) = \begin{pmatrix} 2\pi & 0 \\ \frac{\partial \mathcal{J}_2}{\partial m}\big|_{\mathbf{s}} & \frac{\partial \mathcal{J}_2}{\partial E}\big|_{\mathbf{s}} \end{pmatrix} = \begin{pmatrix} 2\pi & 0 \\ -\theta(\mathbf{s}) & \tau(\mathbf{s}) \end{pmatrix}$$

(with τ and θ, respectively, the period of first return and the rotation angle introduced in Section 4.1.2) is a matrix in GL(2). Its inverse

$$(D\mathcal{J})^{-1} = \frac{\partial(M,H_0)}{\partial(J_1,J_2)} = \frac{1}{2\pi\tau}\begin{pmatrix}\tau & 0\\ \theta & 2\pi\end{pmatrix} = \begin{pmatrix}(2\pi)^{-1} & 0\\ \nu_1 & \nu_2\end{pmatrix}$$

is of prime interest to us here: if action values $\mathbf{j}$ correspond to the regular torus $\Lambda_{\mathbf{s}}$, i.e., if $(m,E)=\mathbf{s}$ equals $\mathcal{J}^{-1}(\mathbf{j})$, then $(D\mathcal{J})^{-1}(\mathbf{j})$ determines the difference in energy–momentum for the neighboring torus which corresponds to the action value $\mathbf{j}+d\mathbf{j}$.

When the realization of the monodromy circuit begins at time t_i, the action values $\mathbf{j}_{\mathrm{I,i}}$ and $\mathbf{j}_{\mathrm{II,i}}$ of particles I and II are such that

$$\mathbf{j}_{\mathrm{I,i}} = \mathcal{J}_\mathrm{i}(\mathbf{s}_{\mathrm{I,i}}) = \mathcal{J}_\mathrm{i}\Big((m,E)_{\mathrm{I,i}}\Big)$$

$$\mathbf{j}_{\mathrm{II,i}} - \mathbf{j}_{\mathrm{I,i}} = d\mathbf{j}_\mathrm{i} = D\mathcal{J}_\mathrm{i}\begin{pmatrix}\delta_m\\ 0\end{pmatrix} = \begin{pmatrix}2\pi\\ \frac{\partial\mathcal{J}_2}{\partial m}\end{pmatrix}\delta_m$$

Here and later we imply that derivative $D\mathcal{J}$ is computed in $\mathbf{s}_{\mathrm{I,i}}$ for the map $\mathcal{J}=\mathcal{J}_\mathrm{i}$ defined at time t_i. Under ideal perturbations X_1^Γ and X_1^{placebo}, action values $\mathbf{j}$ for I and II evolve at the same rate and therefore $d\mathbf{j}_\mathrm{f} = d\mathbf{j}_\mathrm{i} = d\mathbf{j}$. At time t_f, they reach their final values $\mathbf{j}_{\mathrm{I,f}}$ and $\mathbf{j}_{\mathrm{II,f}} = \mathbf{j}_{\mathrm{I,f}} + d\mathbf{j}_\mathrm{f}$ such that

$$\mathcal{J}_\mathrm{f}^{-1}(\mathbf{j}_{\mathrm{I,f}}) = (m,E)_{\mathrm{I,f}} = (m,E)_{\mathrm{I,i}}$$

while at the same time

$$(m,E)_{\mathrm{II,f}} = (m,E)_{\mathrm{I,f}} + D\mathcal{J}_\mathrm{f}^{-1}d\mathbf{j}$$

and therefore

$$\Delta\mathbf{s}_{\mathrm{II}} = (m,E)_{\mathrm{II,f}} - (m,E)_{\mathrm{II,i}} = D\mathcal{J}_\mathrm{f}^{-1}d\mathbf{j} - D\mathcal{J}_\mathrm{i}^{-1}d\mathbf{j}$$

Note that here we are careful to distinguish the initial $\mathcal{J}_\mathrm{i}$ and final $\mathcal{J}_\mathrm{f}$ definitions of local actions as well as their respective values $\mathbf{j}_\mathrm{i}$ and $\mathbf{j}_\mathrm{f}$ because $\mathcal{J}$ is multivalued. As we return to $\mathbf{s}_{\mathrm{I,i}}$, local actions do not come back to their initial definition and their final values do not necessarily equal the initial values (cf. Section 3.1). More specifically, $\mathcal{J}_1 \equiv 2\pi m$ is defined globally on D^* and is single valued, while $\mathcal{J}_2(m,E)$ can be approximated near $\mathbf{s}=0$ [24] as

$$\mathcal{J}_2(m,E) \approx E + E\tau(m,E) - m\theta(m,E) + \cdots \tag{41}$$

where τ and θ are given in Eqs. (24b) and (25b), respectively, and $0 < |E+im| \ll \rho_{\max}^2/2$. Using different leaves of the multivalued part $m\arg(E+im)$ of this function results in different choices of $\mathcal{J}_2$.

For a placebo circuit which does not encircle $\mathbf{s}=0$ (Fig. 10, left), smooth actions $\mathcal{J}$ can be chosen globally as real single-valued functions so that the whole placebo circuit remains within one leaf of $\mathcal{J}_2$ in (41). Then, obviously, $\mathcal{J}_\mathrm{f}=\mathcal{J}_\mathrm{i}$ and $\mathbf{s}_{\mathrm{II,f}} = \mathbf{s}_{\mathrm{II,i}}$, i.e., II also returns back to its initial torus. Note that the choice of the leaf is dictated by the smooth continuation of the value of $\mathcal{J}_2$ and can be best seen when particle II passes close to $\mathbf{s}=0$ where $\mathcal{J}_2$ varies steeply with m and other leaves come close.

On the other hand, $\mathcal{J}_\mathrm{f}$ and $\mathcal{J}_\mathrm{i}$ will differ for the monodromy circuit Γ. From (16) we deduce that the respective inverse Jacobian matrices at $(m,E)_{\mathrm{I,i}}$ transform as

$$D\mathcal{J}_\mathrm{i}^{-1} = D\mathcal{J}_\mathrm{f}^{-1}\begin{pmatrix}1 & 0\\ -1 & 1\end{pmatrix}$$

and therefore

$$D\mathcal{J}_\mathrm{f}^{-1} = D\mathcal{J}_\mathrm{i}^{-1}\begin{pmatrix}1 & 0\\ -1 & 1\end{pmatrix}^{-1} = D\mathcal{J}_\mathrm{i}^{-1}\begin{pmatrix}1 & 0\\ 1 & 1\end{pmatrix}$$

Then the final shift in the energy–momentum for II is

$$\Delta\mathbf{s}_{\mathrm{II}} = D\mathcal{J}_\mathrm{i}^{-1}\left[\begin{pmatrix}1 & 0\\ 1 & 1\end{pmatrix} - 1\right]d\mathbf{j}_\mathrm{i} = D\mathcal{J}_\mathrm{i}^{-1}\begin{pmatrix}0\\ dj_1\end{pmatrix} = 2\pi D\mathcal{J}_\mathrm{i}^{-1}\begin{pmatrix}0\\ \delta_m\end{pmatrix} = \frac{2\pi}{\tau}\begin{pmatrix}0\\ \delta_m\end{pmatrix}$$

This explains why the trajectory II does not return to the same torus, but ends up on a torus with the same momentum $m_{\mathrm{II,f}} = m_{\mathrm{II,i}}$ and with energy $E_{\mathrm{II,f}}$ shifted up by $2\pi\delta_m/\tau(\mathbf{s}_{\mathrm{I},i})$.

6. Conclusion

In [1], considering a very simple system with two degrees of freedom which has monodromy, we asked how this monodromy can be observed in a dynamical process. This question has two parts: (i) what perturbation of the system is required and (ii) what observations and measurements should be made. In [1], we gave the answer to (ii) and presented our major Result 1. The result concerns collective dynamical behavior of a family of trajectories (or 'particles').

We consider a situation in which the initial and final energetically allowed region of configuration space is an annulus. The family of trajectories forms at all times a loop γ in phase space. Initially γ projects into the annulus as a homotopically 'trivial' loop. Under a certain time-dependent perturbation, this loop evolves continuously in time into a topologically different nontrivial final loop that wraps around the forbidden region. (The idea of observing an ensemble of particles is central in this result.)

In this paper we give a more detailed answer to (ii), and we give a complete answer to (i). Specifically, in Section 4.2, we define an perturbation X_1 which we call "ideal" and we characterize a large class of admissible perturbations which are deformations of that ideal perturbing vector field. We prove constructively that such perturbations exist. In particular we show in Appendix A that the perturbation we proposed in [1] was admissible and that in the limit of slowly changing (m, E) it approached our ideal X_1. We demonstrate that for the ideal perturbation, the phenomenon observed in Result 1 is *directly* related to Hamiltonian monodromy, because the connection realized dynamically by the perturbed particles is equivalent to that used for computing monodromy. Furthermore, our Results 2 and 3 present alternative possibilities to observe phenomena related to monodromy.

The main attractive feature of Result 1 is its topological nature. Evolution of 'particles' under admissible perturbations X_1 may differ substantially from the ideal case. Some particles may go astray, they will not belong all to the same torus at the same time and may not come back to the same torus eventually. In spite of these differences, the qualitative transformation of the projected image of the loop will persist.

We hope it is obvious that the phenomena we describe are not limited to the system described by Eq. (1). Sufficiently close to an isolated critical $\mathcal{EM}$-value that represents a focus–focus equilibrium, and is at the origin of monodromy, any system behaves in the same way. Therefore this paper opens the way for practical implementation of admissible realizations of monodromy circuits Γ.

To apply these ideas to an atomic or molecular system, two issues need to be addressed. The loop γ is a Lagrangian manifold, and so it can be part of the framework for semiclassical construction of a wave function. Alternatively, we may think of the initial ensemble of particles as representing an initial quantum wavepacket (cf. [39]). The perturbation X_1 would presumably arise from an electromagnetic field, and then we would be making use of resonances between the light frequency and the frequencies of the motion. Thus, for example, circularly polarized radiation can change the angular momentum, while linearly polarized radiation in resonance with a particular transition might change the energy without changing the component of angular momentum.

We leave to future papers discussion of the precise means of implementing a monodromy circuit for atomic or molecular systems.

Acknowledgments

This work was made possible during 2005–2007 by the visiting professorship program of the Région Nord–Pas-de-Calais and was also supported by the NSF. We also thank *Maison de la recherche en sciences humaines, sociales et juridiques* of the Université du Littoral for support and for permitting the use of one of their offices at the *Palais Impérial*, the historic residence of Napoléon in Boulogne-sur-Mer, for our discussions of monodromy.

Appendix A. A different realization of the monodromy circuit

This Appendix describes a different realization of the monodromy circuit based on an alternative time-dependent perturbation. This method was used in a previous paper [1], and it illustrates the fact that the essential results do not require use of an ideal perturbation.

Consider the vector field which we will call X^{mE}:

$$\frac{d}{dt}\begin{pmatrix} M \\ H_0 \\ Q_m \\ Q_e \end{pmatrix} = \begin{pmatrix} f_m(t) \\ f_e(t) \\ 0 \\ 1 \end{pmatrix} \tag{A.1}$$

where Q_e and Q_m are canonical variables conjugate to energy H_0 in (2) and momentum M in (4), respectively. The advantage of using variables (M, H_0, Q_m, Q_e) in (A.1) is in the simple immediate evolution equations

$$\dot{M} = f_m(t) \quad \text{and} \quad \dot{H}_0 = f_e(t) \tag{A.2a}$$

while, obviously, Q_m and Q_e change in the same way as for the unperturbed system, i.e.,

$$\dot{Q}_m = 0 \quad \text{and} \quad \dot{Q}_e = 1 \tag{A.2b}$$

Wherever the symplectic map

$$\Xi : (x, y, p_x, p_y) \mapsto (M, H_0, Q_m, Q_e) \tag{A.3}$$

is a local diffeomorphism, we can obtain Cartesian phase space trajectories as

$$t \mapsto \Xi^{-1}\left(m(t), E(t), Q_m^0, t + Q_e^0\right)$$

It can be seen that this is simply a trajectory of the unperturbed system whose dynamical parameters (m, E) change with time according to (A.2a).

As usual, nothing comes without a price, and the disadvantage of (M, H_0, Q_m, Q_e) is serious. These variables are defined with respect to the trajectories of the Hamiltonian vector field X_{H_0} which are, typically, not closed. So as a particular unperturbed trajectory coils infinitely around $\Lambda_{m,E}$, the origin of $(Q_m,\ Q_e)$ coordinates on $\Lambda_{m,E}$ jumps discontinuously every time the particle encounters the wall at $\rho = \rho_{\max}$. This jump is not related to the hard wall; it is an intrinsic property of these coordinates that would occur also for a soft wall. This makes reconstruction of the geometry of a continuous loop that a family of particles form at any given time t more difficult than the method given in the main text (Eq. (36)). However, trajectories of individual particles perturbed by X^{mE} in Eq. (A.1) can be computed quite easily numerically by taking unperturbed trajectories with certain initial conditions and letting parameters (m, E) vary. While running such 'perturbed' trajectories, we detect the encounters with the wall, reverse the radial momentum, and use Eq. (A.3) to find new values of $Q_m^0,\ Q_e^0$, and then continue the trajectory to the next bounce. This process is necessarily numerical, so it is not easy to anticipate what happens to the initial loop of particles. However, since the change shown in Fig. 3 is topological, and since there is everywhere (except at the outer wall) a *local* diffeomorphism between $\mathbf{j},\ \mathbf{w}$ and (M, H_0, Q_m, Q_e) we expect that the same topological change must occur using the flow X^{mE}.

This is the method that we used in [1]. In the rest of this appendix, we show in detail the relationship between these two methods.

Any phase-space point on any torus $\Lambda_{m,E}$ can be identified by noncanonical coordinates (m, E, ϕ^0, ξ^0) as

$$\mathbf{u} = S_M^{\phi^0} S_{H^0}^{\xi^0 \tau(m,E)} \mathbf{u}_0(m, E) \tag{A.4a}$$

with

$$-\frac{1}{2} \leqslant \xi^0 \leqslant \frac{1}{2} \quad \text{and} \quad 0 \leqslant \phi^0 < 2\pi \tag{A.4b}$$

Unperturbed evolution of any such point between bounces is given by

$$\mathbf{u}(t) = S_M^{\phi^0} S_{H^0}^{t+\xi^0\tau(m,E)} \mathbf{u}_0(m,E) \tag{A.5a}$$

with the restriction on t

$$|t + \xi^0\tau(m,E)| < \frac{1}{2}\tau(m,E) \tag{A.5b}$$

For $\phi^0 = 0,\ \xi^0 = 0$, and $|t| < \tau(m,E)/2$, Eqs. (A.5) define on each torus the set of reference orbits illustrated (for $E > 0$) in Fig. 5 left.

Initial conditions are obtained by setting $\phi^0 = 0,\ t = 0,\ m = m_i = 0,\ E = E_i$, and

$$\mathbf{u}_0(m=0,E) = \left(\sqrt{-2E_i}, 0, 0, 0\right)^T \tag{A.6}$$

and selecting a collection of (for example equally spaced) values ξ_n^0 restricted by (A.4b). The perturbed evolution of the nth trajectory up to its first bounce is given by

$$\mathbf{u}_n(t) = S_{H_0}^{t+\xi_n^0\tau(0,E_i)} \mathbf{u}_0(m,E) \tag{A.7}$$

Bounce conditions are implemented as follows. On the nth trajectory we monitor the value of $\rho(t)$, and when it reaches $\rho_{\max}$ for the kth time, we record the time t, the azimuthal position of the particle ϕ_n^k, and the instantaneous values (m_n^k, E_n^k); from these we compute the corresponding values of the period of first return $\tau_n^k = \tau(m_n^k, E_n^k)$, and the rotation angle $\theta_n^k = \theta(m_n^k, E_n^k)$. Then the nth trajectory continues up to bounce $k+1$ as

$$\mathbf{u}_n(t) = S_M^{\phi_n^k + \theta_n^k/2} S_{H_0}^{t-(t_n^k+\tau_n^k/2)} \mathbf{u}_0(m(t), E(t)) \tag{A.8}$$

Between bounces, the particle moves along its instantaneous torus according to S_{H_0}, but simultaneously it slips from one torus to another according to the change in $\mathbf{u}_0(m(t), E(t))$.

To understand this, it is helpful to consider the function

$$\mathbf{u}_n(t,t') = S_M^{\Phi} S_{H^0}^{t-T} \mathbf{u}_0(m(t'), E(t')) \tag{A.9}$$

Here the unperturbed evolution along each torus is contained in variable t, while the travel from one torus to another is contained in variable t'. If we hold t' fixed, and allow t to vary, then the parameter T is the time t at which the pericenter is reached, and the parameter Φ is the angular location of the point at that time, i.e. the argument of the pericenter. If we hold t fixed and allow t' to evolve, then the particle moves from a point on one torus to points on other tori in such a way that the argument

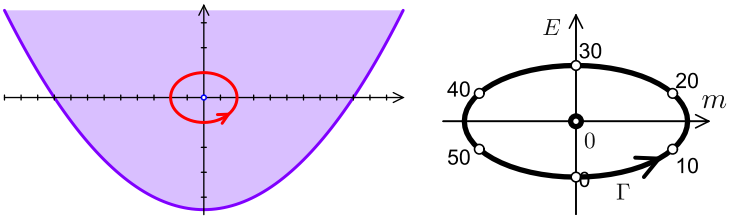

Fig. A.1. Monodromy circuit Γ defined by Eq. (A.10) in the set of regular (m,E)-values of the 'static' system described by the Hamiltonian H_0 in (2) with parameters in (3) (left).

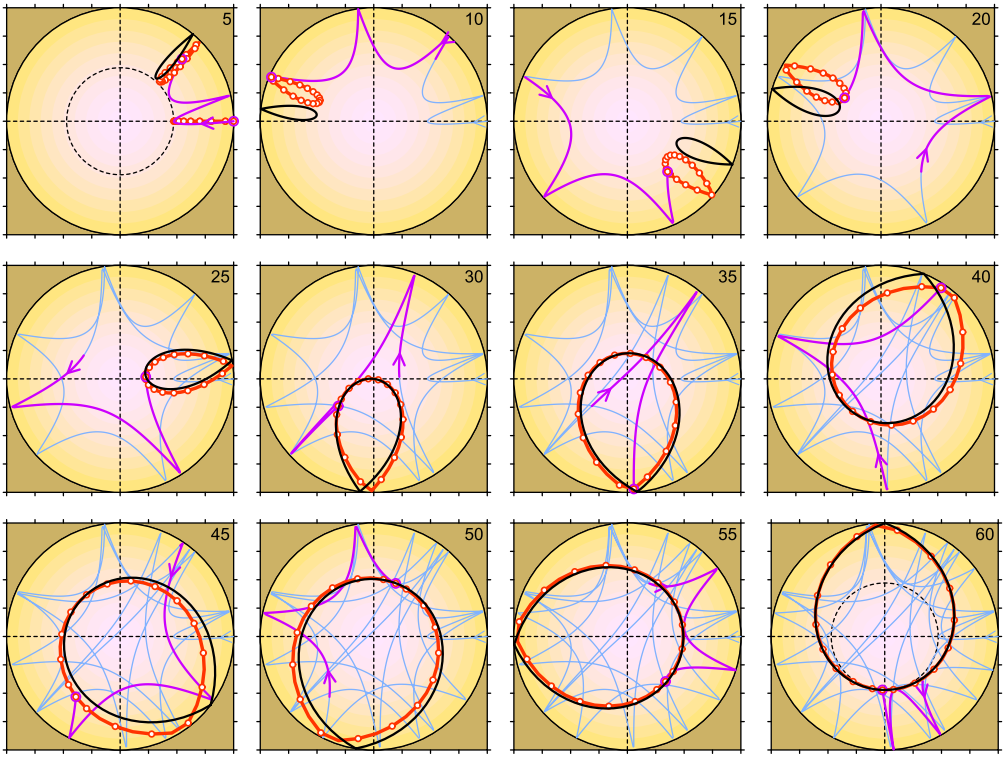

Fig. A.2. The (x,y) plane projection of the trajectory of a particle whose motion is governed by the Hamiltonian in (6) and (A.1) according to propagation Eq. (A.8), and whose unperturbed energy E and momentum m evolve with time $t = 0' \ldots 60'$ according to the monodromy circuit in Fig. A.1 and Eq. (A.10). At time $t = 0'$, the particle starts with $(m,E) = (0,-1)$ on the half-line $\{x > 0, y = 0\}$ at the outer turning point (with $x = \rho = \rho_{\max}$); at time $t = 60'$ it regains $(m,E) = (0,-1)$. Dashed central circle marks the classically forbidden region for this initial–final (m,E). Organization of the figure is similar to that of Fig. 3. Instantaneous positions of other particles in the same family started with the same $m(0) = 0$ and $E(0) = -1$ at different places on $\{x > 0, y = 0\}$ are displayed for each $t = 0', 5', \ldots, 60'$ by empty circles which are joined in the continuous loop (bold line). Also shown (solid closed loop without circle marks) is the evolution along the same circuit Γ of cycle $\gamma_2(t)$ defined in Section 4.3.

of the pericenter and the time required to reach the pericenter do not change. With $t = t'$ in (A.9), the particle moves along the tori by its evolution under H_0, and across the continuum of tori subject to the above restriction: between bounces, the argument of the pericenter and the time required to reach the pericenter do not change.

In Figs. A.1–A.3, we compare this method to the one in the main body of the paper. Similar to Section 4.2, we set $t_i = 0$, $t_f = 60$, $\Omega = 2\pi/60$, and $\mathbf{s}(t_i) = \mathbf{s}(t_f) = (0,-1)$, and fix other parameters (2) by Eq. (3). However, we use a slightly different parameterization

$$\Gamma : [0,60] \to \mathbb{R}^2 : t \mapsto \mathbf{s}(t) = \begin{pmatrix} 2\sin\Omega t \\ -\cos\Omega t \end{pmatrix} \tag{A.10}$$

for our computations in this appendix. The difference from the monodromy circuit used before (see (7) and Fig. 2) is due to historical reasons and is not essential.

Fig. A.1 shows that similar to the circuit in Fig. 2, the circuit defined in (A.10) is situated well within the set of regular $\mathcal{EM}$-values while encircling the origin $(m,E) = 0$. Comparing to (A.2a), we can see that

$$f_m(t) = 2\Omega\cos\Omega t \quad \text{and} \quad f_e(t) = \Omega\sin\Omega t$$

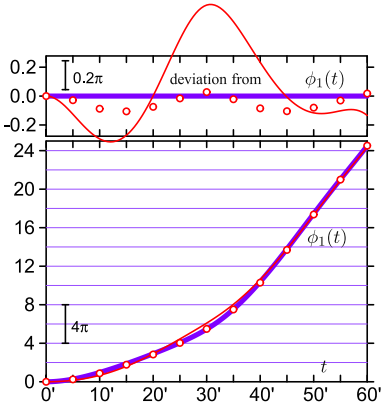

Fig. A.3. Numerical data (empty circles) on the azimuthal angle ϕ of the singular tip of the loop of the instantaneous positions of a family of particles evolving under the realization of the monodromy circuit Γ in Eq. (A.10) and Fig. A.1 based on X^{mE} in (A.1) (cf. Fig. A.2). Evolution of the local angle variable $\phi_1(t)$ for the ideal realization of the same circuit based on the continuous family of cycles $[\gamma_2]$ in (30); exact values of $\phi_1(t)$ and those based on asymptotic expressions (24b) and (25b) are shown by bold and fine solid lines, respectively. The top plot shows the difference between $\phi_1(t)$, its approximation, and numerical data for the X^{mE} evolution.

Since the monodromy circuit Γ in (A.10) and Fig. A.1 differs from that in Section 4.3 [see (7) and Fig. 2], and quantitative comparison to Fig. 3 is not possible, we used the propagation (36) to compute and plot in Fig. A.2 the **q**-space image of $\gamma_2(t)$ (solid line without circle marks) obtained for Γ in (A.10) and Fig. A.1 under the ideal perturbation X_1 defined by the continuous family of cycles $[\gamma_2]$ (30).

As one can expect, since the two realizations differ, the shape and position of the loops produced in **q**-space by different propagators are not the same. However, they are close enough. The main point to observe is that our Result 1 holds perfectly. The initial ρ-loop evolves into a topologically different loop which belongs clearly to the class $[\gamma_2(0') - \gamma_1]$. Furthermore, Result 2 can be confirmed as well. This means that the realization which is based on X^{mE} is admissible. Indeed, the perturbing vector field X^{mE} generates a "near ideal" flow in the sense that at each instant t, all particles are on one torus $\Lambda_{m(t),E(t)}$. However, the evolution of angles from one torus to another differs in the two methods. This example illustrates that many different evolutions will give the same topological result.

References

[1] J.B. Delos, G. Dhont, D.A. Sadovskiĭ, B.I. Zhilinskiĭ, Europhys. Lett. 83 (2008) 24003.

[2] For all $\mu > 0$ and $a > 0$ we can do this without any loss of generality. Using the standard linear symplectic scaling

$$(\mathbf{q}, \mathbf{p}) \mapsto (\lambda^{-1}\mathbf{q}', \lambda\mathbf{p}')$$

where $\lambda = \sqrt{a\mu}$ and rescaling time by $\omega = \sqrt{a/\mu} > 0$, we can always express the unperturbed Hamiltonian in (2) in the form

$$H_0(\mathbf{q}', \mathbf{p}') = \frac{1}{2}\left((\mathbf{p}')^2 - (\mathbf{q}')^2\right), \quad \text{for } |\mathbf{q}'| \leqslant \lambda\rho_{\max}$$

It follows that systems with Hamiltonian in (2) form a family with one parameter $\lambda\rho_{\max}$. It is sufficient to study one representative of this family.

[3] Several other names are often added to this theorem: Nekhoroshev [40] suggests Poincaré and Lyâpunov, while Vũ Ngọc and Nguyên Tiên point out to a similar statement proven by Mineur [41].

[4] In general, the word 'monodromy' is used to describe what happens when something goes once ($\mu o \nu o$) around a circuit ($\delta\rho o\mu o\sigma$). A 'monodromy theorem' in complex analysis states that if a function is analytically continued around a closed circuit in the complex plane not enclosing a branch point, then the function comes back to its original value. The 'monodromy matrix' defined by Poincaré describes small displacements $(\delta p, \delta q)$ from a periodic orbit $(P(t), Q(t))$: on one cycle around the orbit, the final displacements are related to the initial displacements by the monodromy matrix. In the

present paper, the relevant *circuit* is the directed path Γ in the (m,E) plane and *monodromy* is the relationship between final and initial dynamical variables after one circuit.

[5] In this paper, we denote angle and actions as functions $\mathbf{W} = (W_1, W_2)$ and $\mathbf{J} = (J_1, J_2)$, respectively. These functions are defined on $\mathbb{R}^4$ with coordinates $(\mathbf{q},\mathbf{p})$ and have values $\mathbf{w} = (w_1, w_2)$ and $\mathbf{j} = (j_1, j_2)$. By convention, W_1 and W_2 take values w_1 and w_2 in $[0,1]$. It is also sometimes convenient to use angles $\phi_{1,2} = 2\pi w_{1,2}$ and the corresponding conjugate actions $I_{1,2} = J_{1,2}/(2\pi)$. The first action J_1 is defined *globally* for all (m,E) as the angular momentum M in (4) times 2π. However, the conjugate angle W_1 is, generally, not simply the polar angle factor 2π. (This happens only for $m = 0$.) The second action J_2 is a multivalued function whose value j_1 can be obtained by integrating $\mathbf{p}\,d\mathbf{q}$ along γ_2.

[6] For brevity and with some abuse of standard definitions, we call cycles concrete directed fundamental loops γ_1, γ_2, etc. Rigorously, cycles are classes $[\gamma_1]$, $[\gamma_2]$, etc, of homotopy or homology equivalent loops which form the basis of the fundamental group π_1 or homology group H_1, respectively.

[7] Following conventional usage in physics, we also use the word 'action' to mean the action integral $\mathcal{J}_k$, which is the value of J_k computed by integration along the cycles γ_k on tori $\Lambda_{(m,E)}$ and thus parameterized by the values of momentum m and energy E. If one considers $\mathcal{EM}^{-1}$ as a "multivalued map", then $\mathcal{J}_k(m,E)$ can be seen as a pullback of J_k by $\mathcal{EM}^{-1}$, i.e., $\mathcal{J}_k = J_k \circ \mathcal{EM}^{-1}$.

[8] J.J. Duistermaat, Commun. Pure Appl. Math. 33 (1980) 687.

[9] R.H. Cushman, J.J. Duistermaat, Bull. Am. Math. Soc. 19 (1988) 475.

[10] S. Vũ Ngọc, Commun. Math. Phys. 203 (1999) 465.

[11] D.A. Sadovskií, B.I. Zhilinskií, Phys. Lett. A 256 (1999) 235.

[12] L. Grondin, D.A. Sadovskií, B.I. Zhilinskií, Phys. Rev. A 65 (2002) 012105.

[13] B.I. Zhilinskií, Acta Appl. Math. 87 (2005) 281.

[14] B.I. Zhilinskií, Hamiltonian monodromy as lattice defect, in: Topology in Condensed Matter, Springer Series in Solid-State Sciences, vol. 150, Springer Verlag, Berlin, 2006, pp. 165–186.

[15] L.M. Bates, R.H. Cushman, Global Aspects of Classical Integrable Systems, Birkhäuser, Basel, 1997.

[16] R.H. Cushman, D.A. Sadovskií, Europhys. Lett. 47 (1999) 1;
R.H. Cushman, D.A. Sadovskií, Physica D 142 (2000) 166;
K. Efstathiou, R.H. Cushman, D.A. Sadovskií, Physica D 194 (2004) 250;
K. Efstathiou, D.A. Sadovskií, B.I. Zhilinskií, Proc. R. Soc. Ser. A 463 (2007) 1771;
C.R. Schleif, J.B. Delos, Phys. Rev. A 76 (2007) 013404;
C.R. Schleif, J.B. Delos, Phys. Rev. A 77 (2008) 043422;
C.R. Schleif, J.B. Delos, Phys. Rev. A 78 (2008) 049903;
K. Efstathiou, O.V. Lukina, D.A. Sadovskií, Phys. Rev. Lett. 101 (2008) 253003.

[17] R.H. Cushman, H.R. Dullin, A. Giacobbe, D.D. Holm, M. Joyeux, P. Lynch, D.A. Sadovskií, B.I. Zhilinskií, Phys. Rev. Lett. 93 (2004) 024302;
A. Giacobbe, R.H. Cushman, D.A. Sadovskií, B.I. Zhilinskií, J. Math. Phys. 45 (2004) 5076.

[18] M.S. Child, T. Weston, J. Tennyson, Mol. Phys. 96 (1999) 371;
N.F. Zobov, S.V. Shirin, O.L. Polyansky, J. Tennyson, P.-F. Coheur, P.F. Bernath, M. Carleer, R. Colin, Chem. Phys. Lett. 414 (2005) 193.

[19] I.N. Kozin, R.M. Roberts, J. Chem. Phys. 118 (2003) 10523.

[20] C.A. Arango, W.W. Kennerly, G.S. Ezra, Chem. Phys. Lett. 392 (2004) 486;
C.A. Arango, W.W. Kennerly, G.S. Ezra, J. Chem. Phys. 122 (2005) 184303.

[21] Note that the additional $m \to -m$ symmetry is present in many axially symmetric physical systems and is often reduced so that only $m \geqslant 0$ is considered. In this case, the line $\{m = 0\}$ in the (m,E) plane represents a stratum of nongeneric energy–momentum values and the singularity of $\mathcal{J}_2$ on this line is justifiable. Breaking the $m \to -m$ symmetry removes any specifics of $\{m = 0\}$ and thus any reason for action integrals and other functions of (m,E) describing a generic system to be singular or even to have extrema on this line.

[22] Regular, critical, and singular points. Consider an integrable Hamiltonian system on the phase space $T\mathbb{R}^2 \sim \mathbb{R}^4$ with standard symplectic coordinates $\mathbf{u} = (\mathbf{q},\mathbf{p})$. Let (M,H) be its two first integrals (conserved quantities) in involution which define the map $\mathcal{EM}$ in Section 3.3. A point $\mathbf{u} \in \mathbb{R}^4$ is a *regular point* of $\mathcal{EM}$, if the gradients of M and H are linearly independent at $\mathbf{u}$. Otherwise $\mathbf{u}$ is a *critical point* of $\mathcal{EM}$. A point (m,E) in the range $\mathsf{R} \subseteq \mathbb{R}^2$ of $\mathcal{EM}$ (a 2-domain in $\mathbb{R}^2$) is a *regular value* of $\mathcal{EM}$ if all points in its preimage $\mathcal{EM}^{-1}(m,E) \subset \mathbb{R}^4$ are regular. Otherwise (m,E) is a *critical value*. The dimension of preimages of regular values, or *regular fibers*, is 2; preimages of critical values, or *critical fibers*, can have lesser dimension. Critical points are not necessarily singular points of either one or both Hamiltonian vector fields X_H and X_M. If a connected component $\Lambda \subseteq \mathcal{EM}^{-1}(m,E)$ has nonzero dimension and contains an *isolated* critical point $\mathbf{u}$, the latter is a singular point of Λ. For our system (see Section 3.2), $(0,0) \in \mathbb{R}^2$ is an isolated critical value, its preimage $\mathcal{EM}^{-1}(0,0) \subset \mathbb{R}^4$ is a connected two-dimensional critical fiber $\Lambda_{(0,0)}$ [23] with one singular point at the origin $0 \in \mathbb{R}^4$, which is an unstable equilibrium of the system.

[23] The topology of the regular combined level set of (M,H_0) is that of a cylinder, i.e., a direct product $[0,1] \otimes \mathbb{S}^1$, cf. Fig. 7. The topology of the singular level (0,0) is that of two cones with a common vertex at $p = q = 0$, i.e., a cylinder with a single internal basis circle pinched to a point. Due to the hard wall reflection at $\rho = \rho_{\max}$ we can recover 'tori' of the system with Hamiltonian (2) by identifying points on the two edges of the cylinder. With this identification, all trajectories are continuous. To distinguish such varieties from the tori $\mathbb{T}^2$ and the pinched torus, we sometimes use quotes. Note that the hard wall may be regarded as the limit of a steep but continuous confining potential energy function (such as "Mexican hat" or "champagne bottle" potential $V(\mathbf{q}) = -\frac{1}{2}a\mathbf{q}^2 + b\mathbf{q}^4$). Then each our 'torus' becomes a limit for regular tori $\mathbb{T}^2$.

[24] S. Vũ Ngọc, Topology 42 (2003) 365.

[25] M. Symington, Four dimensions from two in symplectic topology, in: G. Matic, C. McCrory (Eds.), Topology and Geometry of Manifolds, Proc. Symp. Pure Math. no. 71, Am. Math. Soc., Providence, RI, 2003, pp. 153–208.

[26] R.H. Cushman, J.J. Duistermaat, J. Diff. Eqs. 172 (2001) 42.

[27] An open punctured 2-disk $D^* = D \setminus (0,0)$ is homotopic to $\mathbb{S}^1$. So like $\pi_1(\mathbb{S}^1)$, the fundamental group $\pi_1(D^*)$ is isomorphic to $\mathbb{Z}$. This group is generated by the homotopy class $[\Gamma]$ of the nontrivial path Γ in (7).

[28] The origin of angle coordinates on each torus is arbitrary, and should be chosen so that on a smooth path in phase space from one torus to another the angle variables change smoothly. We choose the origin of angle coordinates on each torus so that at the outermost point $|\mathbf{q}| = \rho_{\max}$ with $y = 0$, i.e., with $\phi = 0$, we have $w_1 = 0$ and $w_2 = -1/2$.

[29] No Polar Coordinates, Lectures by Richard Cushman, prepared by K. Efstathiou and D.A. Sadovskií, in: J. Montaldi, T. Ratiu (Eds.), Geometric Mechanics and Symmetry, The Peyresq Lectures, London Math. Soc. Lect. Note Ser. no. 306, Cambridge University Press, Cambridge, UK, 2005.

[30] Note that $D\mathcal{J}(m,E) \in \mathrm{GL}(2)$ for any regular (m,E), i.e., for all (m,E) in $\mathbb{R} \setminus (0,0)$.

[31] K. Efstathiou, M. Joyeux, D.A. Sadovskií, Phys. Rev. A 69 (2004) 032504.

[32] N.N. Nekhoroshev, D.A. Sadovskií, B.I. Zhilinskií, C. R. Acad. Sci. Paris I 335 (2002) 985;
N.N. Nekhoroshev, D.A. Sadovskií, B.I. Zhilinskií, Ann. Henri Poincaré 7 (2006) 1099.

[33] Eq. (27d) can be used to continue the reference orbits along multiple circuits about the monodromy center (0,0).

[34] The class $[\gamma]$ of equivalent directed loops γ is called a *cycle*. In the first homology group H_1 and in the fundamental group π_1, the equivalence of loops is established using homology and homotopy, respectively. Any particular loop γ is a cycle representative. For brevity, we call γ a cycle when we consider properties of the whole family of such loops. Regular fibers $\Lambda_{(m,E)}$ of our system are tori [23] and their groups H_1 and π_1 are isomorphic to an abstract lattice $\mathbb{Z}^2$ called the *period lattice*. The elementary cell of this lattice is shown, for example, in Fig. 8. By a cycle $[\gamma]$ we will typically imply a homology cycle which is needed to study monodromy (see Section 3.3).

[35] The loop γ_2, (which we construct explicitly in (30) of Section 4.1.4) corresponds to the orbits of the flow of the Hamiltonian vector field X_{J_2} of the local action J_2. (It is uniquely determined up to a $\mathrm{SL}(2,\mathbb{Z})$ transformation of $([\gamma_1],[\gamma_2])$ and (J_1,J_2).) From this point of view, this cycle basis $([\gamma_1],[\gamma_2])$ of $H_1(\Lambda_{(m,E)})$ can be called *dynamical*.One might think that we could use instead of our γ_2 a "*ρ-loop*" which has azimuthal angle ϕ fixed and which begins at $\rho_{\max}$ with p_ρ negative and ends at $\rho_{\max}$ with p_ρ positive [23]. Equivalently, we might wish to intersect tori $\Lambda_{(m,E)}$ by a hyperplane $\{y = 0\}$ in $\mathbb{R}^4$.However, it is precisely this method that produces the "action" variables that have discontinuous derivatives on the half-line $\{m = 0, E \geqslant 0\}$. Action variables computed on such loops do not go smoothly across that line.

[36] At the same time, Eqs. (30), (7), and (24a)–(26) define explicitly the bases $\{[\gamma_1(t)],[\gamma_2(t)]\}$ for the fundamental groups $\pi_1(\Lambda_{\mathbf{s}(t)}), \mathbf{s}(t) = (m(t),E(t))$, with reference point $\mathbf{u}_0(\mathbf{s}(t))$. Because we chose $\mathbf{u}_0(\mathbf{s}(0)) \neq \mathbf{u}_0(\mathbf{s}(60))$, the groups $\pi_1(\Lambda_{\mathbf{s}(0)})$ and $\pi_1(\Lambda_{\mathbf{s}(60)})$ are not the same and we do not have a π_1-bundle over Γ. On the other hand, $H_1(\Lambda_{\mathbf{s}(0)})$ and $H_1(\Lambda_{\mathbf{s}(60)})$ are the same groups with different bases that are related by the monodromy matrix, see also [42].

[37] The fibers $\Lambda_{(m,E)}$ of our system are two-dimensional surfaces in $\mathbb{R}^4$ with coordinates (x,p_x,y,p_y) [23]. They can be embedded (and immersed) in various ways in a space $\mathbb{R}^3$. One possibility for the choice of the coordinates in $\mathbb{R}^3$ is to use (x,y) together with an axially symmetric function, such as the polynomial $K = \frac{1}{2}(xp_x + yp_y) = \frac{1}{2}\rho p_\rho$ or simply the radial component p_ρ of $\mathbf{p}$. This gives a faithful representation of $\Lambda_{(m,E)}$ for all (m,E) *excluding* the open semiaxis $\{m = 0, E > 0\}$.

[38] One might wish that the perturbing vector field X_1, such as the one in (34), is Hamiltonian. Formally, we might write a Hamiltonian H_1 that defines such a vectorfield as a continuous function depending *only* on local angles $\mathbf{w}$ and time t. Then the full Hamiltonian is

$$H = H_0(\mathbf{j}) + H_1(\mathbf{w},t)$$

where the perturbation

$$H_1(\mathbf{w},t) = -c_1(t)w_1 - c_2(t)w_2$$

is *linear* in local angles $\mathbf{w}$. Such a Hamiltonian would produce the desired "ideal" flow. However, since $(\mathbf{q},\mathbf{p})$ are periodic functions of angle variables $\mathbf{w}$, such a Hamiltonian could not be single valued in $(\mathbf{q},\mathbf{p})$. If instead we insist that it must be single valued in $(\mathbf{q},\mathbf{p})$, then it must be periodic in $\mathbf{w}$. However, there is no need to insist on the form or even the existence of any such H_1: the value of H is not conserved, and is not important. What matters is that at the instantaneous phase space location of any particle, the flow is similar to that produced by (34) at that location. In other words, only local phase-space gradients of H_1 (i.e., the vector field X_1) matter.

[39] M. Sanrey, M. Joyeux, D.A. Sadovskií, J. Chem. Phys. 124 (2006) 074318.

[40] N.N. Nekhoroshev, Funk. Analiz 28 (1994) 3.

[41] H. Mineur, J. Ecole Polytech. Ser. III 143 (1937) 173;
H. Mineur, J. Ecole Polytech. Ser. III 143 (1937) 237.

[42] A. Giacobbe, Diff. Geom. Appl. 28 (2008) 140.